nature cancer

ARTICLES

https://doi.org/10.1038/s43018-022-00376-z

Check for updates

OPEN

A local human Vδ1 T cell population is associated with survival in nonsmall-cell lung cancer

Yin Wu[1,2,3,4,55]✉, Dhruva Biswas[1,2,5,55], Ieva Usaite[1], Mihaela Angelova[2], Stefan Boeing[6], Takahiro Karasaki[1,2], Selvaraju Veeriah[1], Justyna Czyzewska-Khan[1], Cienne Morton[3], Magdalene Joseph[3,4], Sonya Hessey[1,7], James Reading[1,8], Andrew Georgiou[1,8], Maise Al-Bakir[2], TRACERx Consortium*, Nicholas McGranahan[1,9], Mariam Jamal-Hanjani[1,7], Allan Hackshaw[10], Sergio A. Quezada[1,8], Adrian C. Hayday[3,4]✉ and Charles Swanton[1,2]✉

Murine tissues harbor signature γδ T cell compartments with profound yet differential impacts on carcinogenesis. Conversely, human tissue-resident γδ cells are less well defined. In the present study, we show that human lung tissues harbor a resident Vδ1 γδ T cell population. Moreover, we demonstrate that Vδ1 T cells with resident memory and effector memory phenotypes were enriched in lung tumors compared with nontumor lung tissues. Intratumoral Vδ1 T cells possessed stem-like features and were skewed toward cytolysis and helper T cell type 1 function, akin to intratumoral natural killer and CD8⁺ T cells considered beneficial to the patient. Indeed, ongoing remission post-surgery was significantly associated with the numbers of CD45RA⁻CD27⁻ effector memory Vδ1 T cells in tumors and, most strikingly, with the numbers of CD103⁺ tissue-resident Vδ1 T cells in nonmalignant lung tissues. Our findings offer basic insights into human body surface immunology that collectively support integrating Vδ1 T cell biology into immunotherapeutic strategies for nonsmall cell lung cancer.

Immune checkpoint inhibitors (CPIs) have revolutionized the treatment of cancer by providing durable remissions, albeit for a minority of patients. CPIs work, at least in part, by de-repressing tumor (neo)antigen-specific αβ T cells. Thus, many efforts to improve efficacy have focused on this axis[1,2]. Indeed, some utility of tumor mutational burden (TMB)[3,4], presence and quality of CD8⁺ T cells[5,6] and major histocompatibility complex (MHC) class I loss of heterozygosity[7] in predicting responses to CPIs provide collective evidence of the contributions of antigen-specific αβ T cells. Nevertheless, a high TMB does not guarantee responses to CPIs and a lack of MHC-I and/or low TMB does not preclude good responses[8,9].

Alongside αβ T cells, we and others have previously demonstrated that γδ T cells are also found within tumors[10–14]. These cells are evolutionarily conserved, implying a vital and nonredundant role and, although they are often less abundant than αβ T cells, this disparity may be compensated by their polyclonal response potentials compared with the highly clonotypic responses of αβ T cells[15]. Indeed, it is well established that γδ T cells protect against cancer in mice, both independently and synergistically with αβ T cells[16,17], highlighting the need to better assess their importance in human cancers[18,19]. Although such studies have been limited by the availability of technologies to rigorously identify, isolate and examine γδ T cells, a recent in silico study of >5,000 cancer patients demonstrated that, of all 22 immune cell types studied, the intratumoral γδ T cell signature was the trait most significantly associated with remission[10].

Similar to αβ T cells, γδ T cells are also composed of distinct subsets occupying different functional niches. It is clear in the murine setting that body surface tissues in which carcinomas arise harbor signature tissue-specific γδ T cell subsets[20]. We recently demonstrated that human breast epithelium is enriched in the Vδ1 subset of γδ T cells and that these cells possess potent anti-tumor functions, including the capacity to kill transformed cells in vitro and produce tumor-antagonistic cytokines, for example, interferon-γ (IFN-γ)[11]. Moreover, activation of these Vδ1 T cells did not require cognate peptide–MHC but instead the cells responded to conserved signals of tissue stress, via innate receptors, entirely distinct from co-located αβ T cells[11]. In other words, Vδ1 T cells were an independent, but potentially synergistic, population of anti-tumor lymphocytes in the tumor microenvironment (TME). Furthermore, in patients with aggressive triple-negative breast cancers (TNBCs), the intratumoral presence of Vδ1 T cells was more significantly associated with survival than co-located αβ T cells. A subsequent study employing CIBERSORT demonstrated that intratumoral γδ T cells also predicted survival in a larger cohort of 169 patients with TNBCs in the METABRIC dataset[21]. Recent studies have described similar populations of resident Vδ1 T cells in colorectal cancers, where their presence was associated with lower-stage disease[12], and in hepatocellular carcinomas, where the presence of total γδ

[1]Cancer Research UK Lung Cancer Centre of Excellence, University College London Cancer Institute, London, UK. [2]Cancer Evolution and Genome Instability Laboratory, The Francis Crick Institute, London, UK. [3]Peter Gorer Department of Immunobiology, School of Immunology & Microbial Sciences, King's College London, London, UK. [4]Immunosurveillance Laboratory, The Francis Crick Institute, London, UK. [5]Bill Lyons Informatics Centre, University College London Cancer Institute, London, UK. [6]Bioinformatics & Biostatistics and Software Development & Machine Learning Team, The Francis Crick Institute, London, UK. [7]Cancer Metastasis Lab, University College London Cancer Institute, London, UK. [8]Cancer Immunology Unit, Research Department of Haematology, University College London Cancer Institute, London, UK. [9]Cancer Genome Evolution Research Group, University College London Cancer Institute, London, UK. [10]Cancer Research UK & University College London Cancer Trials Centre, University College London, London, UK. [55]These authors contributed equally: Yin Wu, Dhruva Biswas. *A list of authors and their affiliations appears at the end of the paper. ✉e-mail: yin.wu@kcl.ac.uk; adrian.hayday@kcl.ac.uk; charles.swanton@crick.ac.uk

T cells was associated with survival[14]. Thus, we hypothesize that human body surface tissues, similar to their murine counterparts, harbor signature tissue-resident γδ T cells contributing to cancer immunosurveillance.

To test this hypothesis in human lung, we have leveraged samples and clinical data collected from the TRACERx (Tracking non-small-cell lung Cancer Evolution through therapy (Rx)) Study[22]. Nonsmall cell lung cancers (NSCLCs) are cancers of unmet clinical need. Although outcomes are better for patients with early-stage disease, overall outcome is poor with a 5-year survival rate of <20%[23]. These cancers are clearly susceptible to immunosurveillance, as witnessed by instances of successful CPI therapy and evidence of immune editing in treatment-naive primary lung cancers[24]. However, despite harboring high TMBs[25], only a minority of patients with NSCLCs respond to CPI therapy. By employing flow cytometry, quantitative T cell receptor-sequencing (TCR-seq) and RNA-sequencing (RNA-seq), we now find that both nontumor (NT) human lung tissues and NSCLCs harbor resident populations of γδ T cells, particularly enriched in the Vδ1 subtype. Moreover, these Vδ1 T cells possess a T-cytolytic type 1 (Tc1) phenotype that is well established as beneficial to patients with cancer[26–28]. Finally, the presence of Vδ1 T cells in both NT tissue and lung tumors was significantly associated with remission. The former association is of particular interest because cell populations in NT tissue, as opposed to tumors, may be retained in situ postoperatively.

Results

Vδ1 T cells are present in lung epithelium and enriched in NSCLCs. To characterize the T cell landscape in human lung epithelium and NSCLCs, we examined tissue and tumor-infiltrating lymphocytes (TILs) isolated from NT lung tissues and paired tumors of patients with surgically resected NSCLCs collected from the TRACERx Study (Supplementary Table 1). NT tissues were taken as far as possible from tumors at primary surgery and hematoxylin and eosin (H&E)-stained sections examined afterwards by an accredited histopathologist to ensure that samples were tumor free. TILs were isolated by enzymatic digestion and cryopreserved before thawing for use in downstream assays without further manipulation or expansion (see Methods). TILs were immunophenotyped by flow cytometry and absolute T cell counts established using quantitative TCR-seq of region-matched genomic (g)DNA extracted from bulk tissues and tumors (Fig. 1a). Samples were chosen based on the availability of banked TILs and region-matched bulk DNA from patients with at least one follow-up visit after surgical resection (see Methods). Where available, paired contemporaneous peripheral blood mononuclear cells (PBMCs) were also immunophenotyped by flow cytometry to contextualize findings with the well-characterized blood γδ T cell compartment. No other selection criteria were applied.

Similar to their presence in peripheral blood (median, interquartile range (IQR): 2.49%, 0.80–6.76%), γδ T cells detected by flow cytometry comprised a small fraction of total T cells in both NT lung tissues (2.22%, 1.39–5.26%) and tumors (1.15%, 0.85–3.05%), with considerable interindividual variation (Fig. 1b). In contrast to peripheral blood, where most γδ T cells expressed Vδ2, most γδ T cells found in lung tissues and tumors expressed Vδ1 (47.6%, 30.8–74.4% and 46.8%, 32.1–70.0% respectively), consistent with a well-established enrichment of Vδ1 T cells in other tissues[29] (Fig. 1b and Extended Data Fig. 1a,b). Complementary to flow cytometry, we employed quantitative TCR-seq of gDNA at the TCRα/δ (TRA/TRD) locus from matched NT tissues and tumor regions as an independent assay of αβ and γδ T cells, and to assess their absolute numbers per unit of tissue (Fig. 1c). Indeed, there was a strong and significant correlation between the proportion of major Vδ subsets (Vδ1 and Vδ2) detected by flow cytometry and TCR-seq (Extended Data Fig. 1c). We then mapped flow phenotyping proportions (that is, proportion of $CD3^+$ T cells positive for $CD4^+$/$CD8^+$) on to absolute TCR-seq counts of T cells to derive more granular T cell subset numbers (Fig. 1c). Consistent with flow cytometry, TCR-seq also revealed that γδ T cells form a minority subset of total T cells in NT lung tissues (2.70%, 1.30–6.23%) and tumors (1.68%, 0.97–2.60%), and that the Vδ1 subset comprises most of these cells in both NT lung tissues (54.2%, 35.9–76.7%) and tumors (62.0%, 29.5–79.6%) (Fig. 1c). Although NT lung tissues were macroscopically and microscopically tumor free, it was not practical to obtain normal lung tissue from healthy donors to exclude potential effects of tumors on the immune microenvironment of NT lung tissues. To address this issue, we utilized data generated by the Genotype-Tissue Expression (GTEx) project[30], a comprehensive public resource of tissue-specific gene expression from 54 nondiseased tissue sites across almost 1,000 individuals. We found that *TRDC*, a gene expressed by all γδ T cells, was highly expressed in lung tissues compared with other tissue sites (Extended Data Fig. 2a). Furthermore, expression of *TRDV1* (Vδ1 T cells) was higher than *TRDV2* (Vδ2 T cells) within lung tissue (Extended Data Fig. 2b,c), consistent with our own data. Thus, we conclude that γδ T cells, particularly the Vδ1 subset, are present in nonmalignant lung tissue at a steady state.

In many tissues, CD103 has been adopted as a marker of tissue-resident memory (T_{RM}) status, absent on most peripheral blood T cells[31]. Consistent with previous studies, NT lung tissues harbored a $CD103^+CD8^+TCR\alpha\beta$ T_{RM} population (median, IQR: 35.3%, 25.9–55.0%) (Fig. 2a,b)[32,33]. Similar to the $CD8^+$ T cell compartment, we found that many, albeit not all, Vδ1 T cells in NT lung tissues displayed a $CD103^+$ T_{RM} phenotype, particularly in some patients (18.8%, 3.35–62.4%) (Fig. 2a,b). In contrast, most $CD4^+$ and Vδ2 T cells in NT lung tissues were $CD103^-$ as were their counterparts in peripheral blood (Fig. 2a,b). Thus, the resident $CD103^+$ T cell compartment in NT lung tissues mostly comprised $CD8^+$ and Vδ1 T cells.

Compared with NT lung tissues, tumors harbored a greater proportion of $CD8^+$ (median, IQR: 65.6%, 57.7–75.3%), Vδ1 (66.6%, 34.4–78.5%) and Vδ2 T cells (10.3%, 5.03–18.2%) expressing CD103 whereas the proportion of CD103 expressing $CD4^+$ T cells was reduced (Fig. 2b). By mapping flow phenotyping proportions on to TCR-seq counts, we observed significantly greater absolute numbers of $CD8^+$ and Vδ1 T cells with the CD103 phenotype in tumors compared with NT lung tissues; conversely, this was not so for $CD4^+$ and Vδ2 T cells (Fig. 2c).

Intratumoral Vδ1 T cells possess a Tc1 functional phenotype in situ. Intratumoral $CD8^+$ T_{RM} cells have been associated with survival in several cancers[34,35] including NSCLCs[36]. However, the potential contributions of human Vδ1 T cells are less well described and more contentious[37]. Similar to $CD8^+$ αβ T cells, γδ T cells have been operationally classified into effector T cell/memory T cell subsets associated with defined effector functions based on CD45RA and CD27 expression[38]. When we compared Vδ1 T cells in tumors versus NT tissues, we observed an overt shift toward a $CD45RA^-CD27^-$ effector memory T cell (T_{EM}) phenotype by flow cytometry (Fig. 3a,b). Similar to their $CD8^+$ counterparts, Vδ1 T_{EM} cells have been associated with helper type 1 T cell (T_H1 cell) cytokine production (IFN-γ) and cytolysis[38], but whether intratumoral Vδ1 T cells possess this patient-beneficial Tc1 phenotype[27,28] in situ has remained unclear.

To address this, we sorted bulk Vδ1 T cells from disaggregated NT tissues and lung tumors ($n=2$ and $n=5$ patients, respectively) from which there was sufficient material. For comparison, we also sorted, from NT lung tissues and tumors, bulk Vδ2 ($n=3$ and $n=3$ patients), $CD4^+$ ($n=8$ and $n=9$ patients), $CD8^+$ ($n=7$ and $n=9$), and regulatory T cells (T_{reg} cells) ($n=1$ and $n=5$ patients) and natural killer (NK) cells ($n=8$ and $n=7$ patients) (Extended Data Fig. 3a). Disaggregated TILs were immediately frozen and

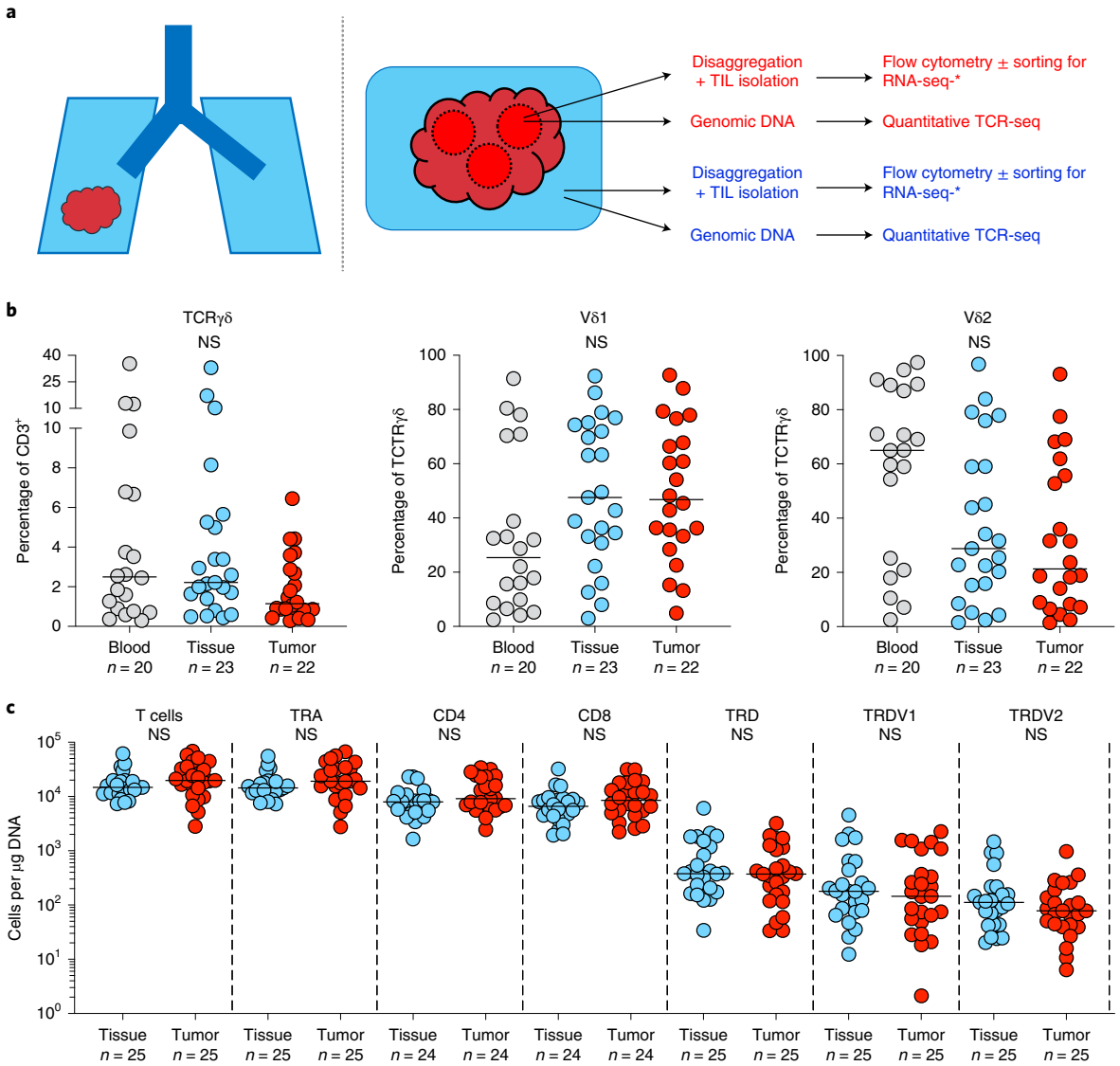

Fig. 1 | Experimental design and γδ T cell composition in lung tissues and NSCLCs. a, Overview of study design. Paired tumor regions (red) and NT lung tissues (blue) collected under the TRACERx Study were enzymatically digested to extract tissue/TILs. TILs were cryopreserved and thawed at a later date for flow cytometry ± RNA-seq. In parallel, gDNA was extracted from undigested matched tumor regions and NT lung tissues and sent for subsequent quantitative TCR-seq. In addition, PBMCs were isolated from contemporaneous blood draws and cryopreserved before subsequent thaw for flow cytometry. **b**, Percentage of $CD3^+$ T cells staining for TCRγδ (left) and percentage of TCRγδ T cells staining for Vδ1 (middle) and Vδ2 (right) in PBMCs (blood), NT lung tissues (tissue) and tumors (tumor). Not all patients had paired samples. The bar represents the median. The Kruskal–Wallis test with post-hoc Dunn's test corrected for multiple testing was used. **c**, Absolute counts of total T cells, αβ T cells (TRA), γδ T cells (TRD) and Vδ1 (*TRDV1*) and Vδ2 (*TRDV2*) T cells per microgram of DNA determined by TCR-seq. Absolute counts of $CD4^+$ αβ T cells (CD4) and $CD8^+$ αβ T cells (CD8) were determined by mapping the proportion of $CD3^+/TCR\gamma\delta^-$ T cells staining for CD4 or CD8 in flow cytometry analysis of paired TILs. No significant differences were observed within demarcated T cell subsets between NT tissues and tumors. Samples with <1 cell μg^{-1} of DNA were not plotted for the purposes of visualization. The bar represents the median. A two-tailed Mann–Whitney *U*-test was used within demarcated T cell subsets. Significant *P* values are shown. NS, not significant. The *n* numbers and datapoints represent independent patients.

subsequently thawed, stained and sorted at 4 °C directly into lysis buffer for RNA-seq, thereby maximizing preservation of the cells' in situ transcriptomes.

Cell types clustered together in a principal component analysis (PCA) of the 500 most variably expressed genes (Extended Data Fig. 3b) and expressed the anticipated canonical lineage markers (Extended Data Fig. 3b). Notably, Vδ1 T cells clustered together with $CD8^+$ T cells and NK cells in this unsupervised analysis (Extended Data Fig. 3b). To determine the functional skew of Vδ1 T cells, we restricted our analysis to canonical transcription factors and effector molecules associated with T cell function and found that intratumoral Vδ1 T cells expressed the T_H1 cell-specific master transcription factor Tbet (*TBX21*) as well as transcripts for granzymes (*GZMs*), perforin (*PRF1*) and IFN-γ (*IFNG*) to levels comparable with those of $CD8^+$ T cells and NK cells (Fig. 3c). Moreover, intratumoral Vδ1 T cells did not express T_H17 cell-associated genes or the T_H17^- cell-specific master transcription factor RORγt (*RORC*). By contrast, these genes were expressed to a variable degree by co-located $CD4^+$ T cells (Fig. 3c). To contextualize the in situ function of intratumoral Vδ1 T cells, we conducted a PCA using these restricted genes of interest expressed by intratumoral Vδ1, Vδ2, $CD4^+$, $CD8^+$ and T_{reg} cells and NK cells. The PCA

demonstrated that intratumoral Vδ1 T cells transciptomically resemble CD8+ T cells and NK cells in function (Fig. 3d). To further contextualize our results, we reanalyzed expression of these genes in comparable cell types isolated from the peripheral blood of healthy volunteers as part of the Blood Atlas Project[39] (Extended Data Fig. 4). Intratumoral Vδ1 T cells resemble peripheral blood γδ T cells in the expression of genes associated with T_H1 cell, T_H2 cell, cytolytic and inhibitory functions. Notably, peripheral blood γδ T cells showed some evidence for T_H17 cell-associated gene expression (Extended Data Fig. 4), whereas this was not seen for intratumoral Vδ1 T cells (Fig. 3c). Most probably, T_H17 cell-associated gene expression in blood reflected the predominance of Vδ2 T cells that have been reported to produce interleukin (IL)-17, albeit rarely[40–42].

Next, we validated the functional potential of intratumoral Vδ1 T cells in vitro by stimulation of TILs with phorbol 12-myristate 13-acetate (PMA) and ionomycin, which mimics TCR signaling. Stimulated TILs were then stained for surface lineage markers and CD107A, a marker of cytotoxic degranulation, as well as for intracellular cytokines. Consistent with their gene expression profile, Vδ1 T cells produced IFN-γ and degranulated on activation (Fig. 3e and Extended Data Fig. 5). Moreover, we could find no evidence of IL-17A production by these cells in contrast to co-located CD4+ T cells (Fig. 3e and Extended Data Fig. 5).

Previous studies have demonstrated that tissue-associated Vδ1 T cells may also be activated by the innate NKG2D receptor without requirement for contemporaneous TCR signaling[11,12,43]. Consistent with an innate, non-TCR/nonclonotypic response mode, we observed no significant clonal focusing of the TCRδ chain in Vδ1 T cells in tumors compared with NT tissues (Extended Data Fig. 6a,b). The gDNA–based TCRγ (TRG) sequencing from bulk tissues is inherently problematic because αβ T cells often harbor productive rearrangements of TRG genes[44]. Nevertheless, RNA-seq of sorted Vδ1 T cells from tumors, albeit in a limited cohort, demonstrated a diverse expression of Vγ chains in most patients, in contrast to Vδ2 T cells which predominantly employed Vγ9 (Extended Data Fig. 6c), further supporting a nonclonal innate response mode for Vδ1 T cells. Moreover, we also observed a positive and significant correlation of the presence of intratumoral Vδ1 T_{EM} cells with region-matched intratumoral expression of transcripts for NKG2D ligands (Fig. 3f).

Intratumoral Vδ1 T cells demonstrate features of tissue residency and stemness. Whereas CD103 expression is often associated with T_{RM} status in T cells[45], this is not always the case[46,47]. Seminal studies by independent teams have collectively established a core transcriptional profile of T_{RM} cells. Specifically, T_{RM} cells upregulate genes associated with tissue retention and homing (*CD69*, *CXCR6*, *ITGAE* and *ITGA1*) and downregulate genes associated with tissue egress (*CCR7*, *S1PR1* and *SELL*) compared with circulating T cells[48,49]. Thus, we compared the expression of these genes in intratumoral Vδ1 and CD8+ T cells, which were predominantly CD103+, versus intratumoral CD4+ T cells, which mostly lacked CD103 (Fig. 2b), and found that this tissue-resident profile was shared by the Vδ1 and CD8+ T cells, consistent with a bona fide T_{RM} status (Fig. 3g and Extended Data Fig. 7).

Recent studies have identified a distinct subset of stem-like memory CD8+ T cells in chronic infection and cancer defined by their expression of the transcription factors/regulators *EOMES*, *TCF7* and *TOX* and the IL-7 receptor (*IL7R*)[50–52]. These cells retain the capacity to proliferate despite chronic inflammatory stimuli and can give rise to highly functional effector cells implicated in tumor control and responses to programmed cell death protein 1 (PD-1) blockade[50,53]. Intratumoral Vδ1 T cells resembled stem-like CD8+ T cells in their expression of *EOMES*, *TCF7* and *TOX* distinct from intratumoral CD4+ T cells (Fig. 3h). Intratumoral Vδ1 T cells also expressed *IL7R* (Fig. 3h), albeit at a somewhat lower level, possibly because these cells are maintained by the epithelial-associated cytokine, IL-15 (ref. [54]).

Presence of Vδ1 T cells predicts ongoing remission in resected NSCLCs. Given that Vδ1 T_{RM} and T_{EM} cells were enriched in tumors relative to NT lung tissues (see above), intratumoral Vδ1 T cells possess a Tc1 phenotype and these cells resemble stem-like CD8+ T cells, we examined their status in relation to clinical outcome in our cohort. Three patients who had incompletely excised primary tumors were excluded from this outcome analysis (Supplementary Table 1). To assess absolute numbers of T_{RM} (CD103+) and T_{EM} (CD45RA−CD27−) cells per unit of tissue/tumor, we mapped flow phenotyping proportions on to TCR-seq counts. Within tumors, the presence of Vδ1 T_{EM} cells was significantly associated with increased relapse-free survival (RFS) whereas this was only a trend for co-located Vδ2, CD4+ and CD8+ T_{EM} cells (Fig. 4a). Importantly, the association of intratumoral Vδ1 T_{EM} cells with improved RFS was not simply a reflection of less advanced disease because we found more intratumoral Vδ1 T_{EM} cells in advanced stages (Extended Data Fig. 8a). Furthermore, we found no association of intratumoral Vδ1 T_{EM} cells with primary tumor size, age, histology or smoking status (Extended Data Fig. 8a). The presence of Vδ1 T_{RM} cells in tumors trended toward association with increased RFS (Extended Data Fig. 8b). Conspicuously, we found the presence of Vδ1 T_{RM} cells in NT tissue to be highly and significantly associated with improved RFS, consistent with an epithelial immunosurveillance role proposed for these cells[16] (Fig. 4b). There was no difference in the number of Vδ1 T_{RM} cells in NT tissue with regard to stage of disease, size of primary, age, histology or smoking status (Extended Data Fig. 8c).

Given the association of Vδ1 T cells in both NT tissues and tumors with ongoing remission, we asked whether such an association might exist for the delta (Δ) of the absolute numbers of Vδ1 T_{EM} cells and Vδ1 T_{RM} cells in NT tissues and paired tumors. No clear association of ΔVδ1 T_{EM} or ΔVδ1 T_{RM} cells with clinical outcome was observed (Extended Data Fig. 8d), suggesting that each subset, that is, intratumoral Vδ1 T_{EM} cells and NT tissue Vδ1 T_{RM} cells, has beneficial impacts independent of the status of their counterpart cells in the reciprocal tissue sites.

To explore further the contributions of tissue-resident Vδ1 T cells, we used the nucleotide sequence of the Vδ1 complementarity -determining region 3 (CDR3) as a molecular fingerprint to track

Fig. 2 | NT lung tissue harbors tissue-resident Vδ1T cells that are enriched in NSCLCs. a, Representative plots of CD103 expression (%) by flow cytometry on Vδ1 (representing $n = 20$, $n = 23$ and $n = 22$ patients for blood, NT tissue and tumor, respectively) and Vδ2 (representing $n = 20$, $n = 23$ and $n = 21$ patients for blood, NT tissue and tumor, respectively), CD4+ (representing $n = 20$, $n = 24$ and $n = 24$ patients for blood, NT tissue and tumor, respectively) and CD8+ T cells (representing $n = 20$, $n = 24$ and $n = 24$ patients for blood, NT tissue and tumor, respectively) were isolated from blood, NT tissue and tumor of one patient. **b**, Summary flow cytometry data of CD103 expression in T cell subsets isolated from blood (Bld), NT tissues (Tis) and tumors (Tum). Not all patients had paired samples. The bar represents the median. A Kruskal–Wallis test with a post-hoc Dunn's test corrected for multiple testing was used. **c**, Absolute counts of CD103+ T_{RM} CD4+, CD8+, Vδ1 and Vδ2 T cells per microgram of DNA from NT tissues and tumors. Samples with <1 cell μg^{-1} of DNA were not plotted for the purposes of visualization. Not all patients had paired samples. The bar represents the median. A two-tailed Mann–Whitney *U*-test was used within demarcated T cell subsets. Significant *P* values are shown. NS, not significant. The *n* numbers and datapoints represent independent patients.

unique Vδ1 T cell clones between NT tissues and paired tumors. On average, approximately a quarter of unique Vδ1 CDR3 sequences present in tumors were found in paired NT tissues (median, IQR: 27.3%, 16.5–35.4%) (Fig. 4c). By contrast, fewer unique TCRα clones present in tumors were also found in paired NT tissues (15.1%, 8.68–19.2%) (Fig. 4d), despite the lower potential for

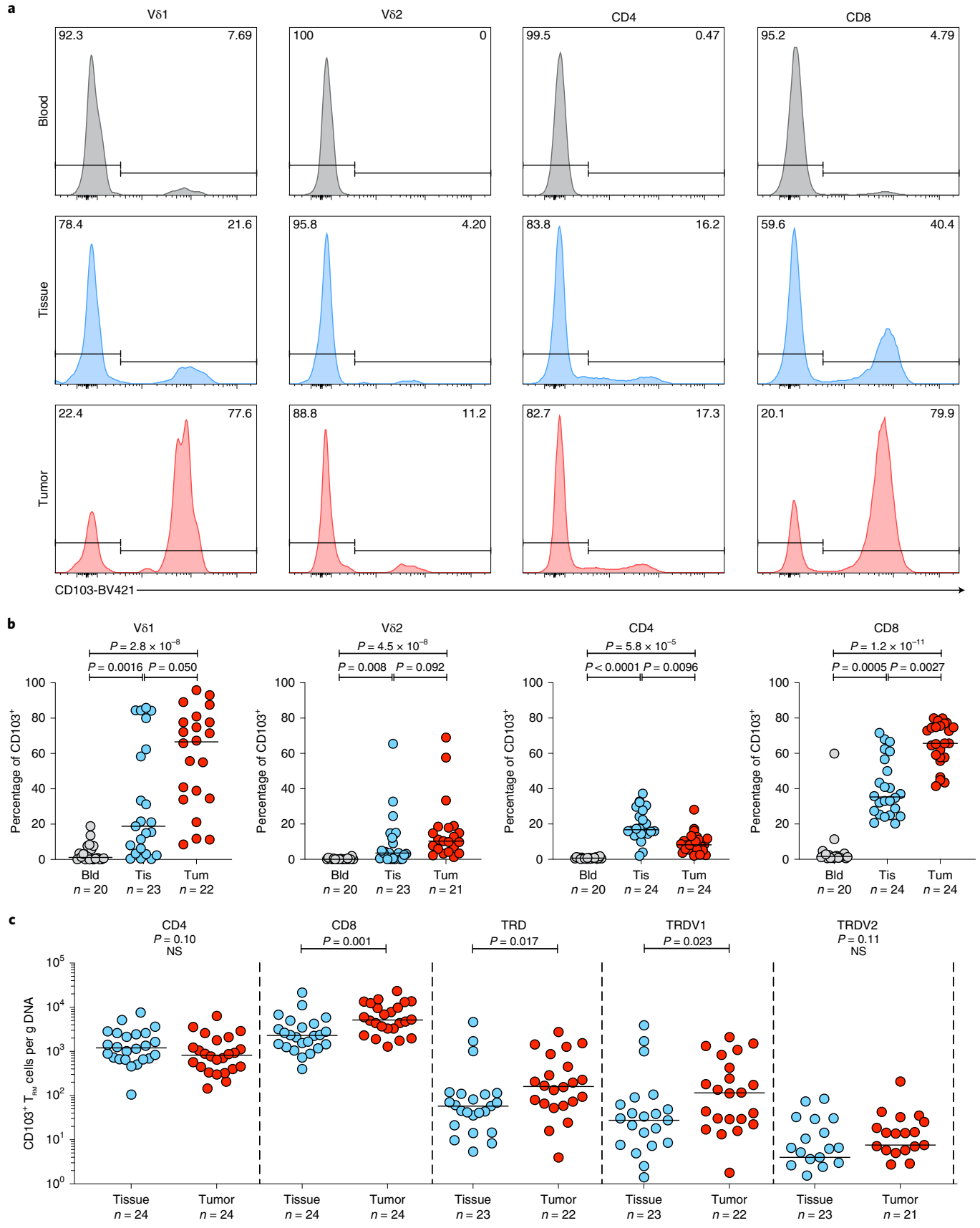

diversity in TCRα compared with TCRδ. Indeed, these data are consistent with a greater proportion of intratumoral αβ T cells (predominantly CD4+) being derived from peripheral blood as opposed to the tissue-resident pool that is the probable source of intratumoral Vδ1 T cells (Fig. 2b). When examined in relation to clinical outcome, patients with a greater proportion of intratumoral Vδ1 T cells also found in paired NT tissues were more likely to remain in remission, consistent with the cells' proposed immunosurveillance function in steady-state tissues (Fig. 4c). Again, this was not the case for the αβ T cell compartment (Fig. 4d).

Acknowledging the limited size of our cohort, we sought to validate our findings in a larger public dataset. The TCRδ locus is excised during TCRα rearrangement in αβ T cells[55]. Thus, we used the expression of *TRDV1* transcripts as a proxy for Vδ1 T cells and *TRDC* transcripts as a proxy for total γδ T cells, thereby assessing the association of these cells with NSCLC survival in The Cancer Genome Atlas (TCGA). Consistent with observations in our own cohort, when split on median expression, we found a significant association of high *TRDV1* expression with favorable overall survival (OS; Fig. 5a), although there was no association with *TRDC* expression (Fig. 5b). Moreover, the improved hazard ratio (HR) in patients with above-median *TRDV1* expression remained significant in multivariate analysis accounting for age, gender, histology, smoking status, stage and *CD4* and *CD8B* gene expression (HR = 0.65, 95% confidence interval (CI) = 0.48–0.88) (Fig. 5c).

Finally, to explore whether there might be a role for Vδ1 T cells with respect to CPI therapy responses, we reanalyzed RNA-seq data from the INSPIRE trial (NCT02644369), a phase II basket clinical trial of pembrolizumab in advanced solid cancers[56]. Using *TRDV1* expression in pre-treatment tumor biopsies as a proxy for intratumoral Vδ1 T cells, we found that patients with above-median expression of *TRDV1* had significantly increased survival compared with those with below-median expression (Fig. 5d). Expression of *TRDC* (pan γδ T cells) was also predictive, although this was probably driven by Vδ1 T cells because the association of *TRDV2* expression (Vδ2T cells) with survival was only a trend (Extended Data Fig. 9). In addition, high expression of *CD4* (CD4+ T cells) did not associate with survival after pembrolizumab whereas high expression of *CD8B* (CD8+ T cells) trended toward association with improved survival (Extended Data Fig. 9).

Discussion

Despite recent advances in immunotherapy, NSCLCs remain a leading cause of cancer-related mortality. Although these cancers are clearly susceptible to immunosurveillance, as evidenced by instances of durable responses to CPI therapy, only a minority of patients benefit. CPIs appear to work, at least in part, by de-repressing tumor (neo)antigen-specific αβ T cells. However, the body surfaces from which carcinomas arise are populated by many other immune cells. These compose organ-specific, tissue-resident immune compartments that collectively include considerably more T cells than the systemic lymphoid organs.

In mice, such compartments commonly include signature populations of tissue-resident γδ T cells seeded during fetal and perinatal development[20]. This is distinct from tissue-resident αβ T cells which arrive later in development, after priming in the lymph nodes as a response to infection[57]. Mice deficient in γδ T cells display heightened susceptibility to de novo cancers[16,58], seemingly more so than mice deficient in αβ T cells[17], establishing a critical and nonredundant role(s) for them. Indeed, these cells appear to be an essential early source of IFN-γ[59], a cytokine pivotal for tumor rejection[26]. In addition to direct effector function, human γδ T cells are also capable of phagocytosis[60,61] and professional antigen presentation to αβ T cells[60,62]. Such sentinel functions, traditionally associated with dendritic cells, are central to activating tumor (neo) antigen-specific αβ T cells and to orchestrating immune responses more generally[63].

Despite apparently advantageous traits, γδ T cell immunotherapies have failed to demonstrate convincing efficacy in solid cancers including in NSCLCs[64]. However, those trials focused exclusively on the Vδ2 subset, the main subset of peripheral blood γδ T cells. By contrast, our assessments of tissue-resident lymphocytes in lung tissues have added to growing evidence that human body surfaces are primarily enriched for Vδ1 γδ T cells. Thus, these cells are well placed to detect malignancy vis-à-vis local/ipsilateral as well as metastatic/contralateral lung cancer recurrences, which comprise a considerable proportion of relapses after surgical resection.

Indeed, an increased presence of Vδ1 T_{RM} cells in NT lung tissues was predictive of ongoing remission in our cohort. Moreover, most Vδ1 T cells found within tumors were also of this tissue-resident phenotype, suggesting an improved capacity for tumor homing and/or retention. Strikingly, a greater proportion of shared Vδ1 T cell clones between tumors and NT tissues was significantly associated with remission in our cohort. Thus, this supports a potential patient-beneficial, cancer immunosurveillance role for human tissue-resident Vδ1 T cells that are present in steady-state NT lung tissues. Although many studies have demonstrated the prognostic utility of intratumoral TILs, these cells clearly cannot actively contribute to immunosurveillance after resection. Conversely, resident immune cells in juxtapositional normal tissues remain in situ at 'ground-zero' where they are well positioned to conduct ongoing cancer immunosurveillance.

Previous studies have demonstrated in vitro that Vδ1 T cells have a Tc1 phenotype[11,12,38,65]. However, given the scarcity of Vδ1

Fig. 3 | Intratumoral Vδ1 T cells have a memory phenotype, are Tc1 skewed and demonstrate features of tissue residency and stemness. a, Representative flow cytometry plots of effector memory status (defined by CD27 and CD45RA expression) of Vδ1 T cells isolated from the NT tissue and tumor of one patient (representing $n = 23$ and $n = 22$ patients for NT tissue and tumor, respectively). **b**, Summary radar plot of effector memory status of Vδ1 T cells isolated from NT tissues ($n = 23$) and tumors ($n = 22$). The median proportion is plotted. A two-tailed Mann–Whitney *U*-test was used between NT tissue and tumor within Vδ1 memory subsets. Significant *P* values are shown. **c**, Expression of T cell master transcription factors and signature effector molecules of lymphocytes sorted directly from tumors grouped into T_H cell, cytolytic and inhibitory modules. Each column represents the denoted cell type from an individual patient. Not all cell types were sorted from matched patients. The color scale denotes the *z*-score of $\log_2(TPM + 1)$ of each gene. **d**, PCA of expression (normalized counts) of genes included in **c** colored by cell type ($n = 9$, $n = 9$, $n = 7$, $n = 5$, $n = 3$ and $n = 5$ patients for CD4+, CD8+, NK, T_{reg}, Vδ2 and Vδ1 cells, respectively). **e**, Violin plots showing intracellular cytokine staining for IFN-γ and IL-17A and cell surface staining for CD107A in Vδ1, CD8+ and CD4+ T cells after in vitro stimulation of bulk TILs ($n = 3$ patients) with PMA and ionomycin (P-I). **f**, Summary data of correlation between region-matched gene expression of NKG2D ligands and absolute numbers of Vδ1 ($n = 14$ patients), Vδ2 ($n = 14$ patients), CD4+ ($n = 15$ patients) and CD8+ ($n = 15$ patients) T_{RM} and T_{EM} cells in tumors. The color scale denotes a two-tailed Spearman's *r*. * denotes significant correlations as follows: *MICA*:Vδ1 T_{EM} $P = 0.027$, *MICB*:Vδ1 T_{EM} $P = 0.031$, *RAET1E*:Vδ1 T_{EM} $P = 0.048$ and *RAET1E*:CD8 T_{EM} $P = 0.045$. **g**, PCA of expression (normalized counts) of core T_{RM} gene signature (*CCR7, CD69, CXCR6, ITGAE, ITGA1, S1PR1* and *SELL*) in Vδ1 ($n = 5$ patients), CD4+ ($n = 9$ patients) and CD8+ T cells ($n = 9$ patients) sorted from tumors. **h**, Expression of genes that define 'stem-like' CD8+ T cells in Vδ1 ($n = 5$ patients), CD4+ ($n = 9$ patients) and CD8+ ($n = 9$ patients) T cells sorted from tumors. The mean ± s.d. is plotted. A Kruskal–Wallis test with post-hoc Dunn's test correction for multiple testing was used. All datapoints represent independent patients.

T cells, many of these studies have relied on ex vivo expansion using cytokine cocktails to achieve requisite numbers for in vitro assays. By using cells sorted directly from NSCLC tumors without ex vivo expansion or in vitro stimulation, we provide corroborating indirect and direct evidence for the in situ function of Vδ1 T cells through flow cytometric immunophenotyping and gene expression analysis. Compared with counterparts in NT lung tissues, Vδ1 T cells isolated from tumors were enriched in the CD45RA$^-$CD27$^-$ T_{EM} subset that has previously been described as potent IFN-γ producers[38]. Moreover, through gene expression analysis and in vitro functional assays, we demonstrate that intratumoral Vδ1 T cells are Tc1 skewed in situ.

Importantly, intratumoral Vδ1 T cells showed no evidence of a possibly tumor-promoting skew toward IL-17. Potentially

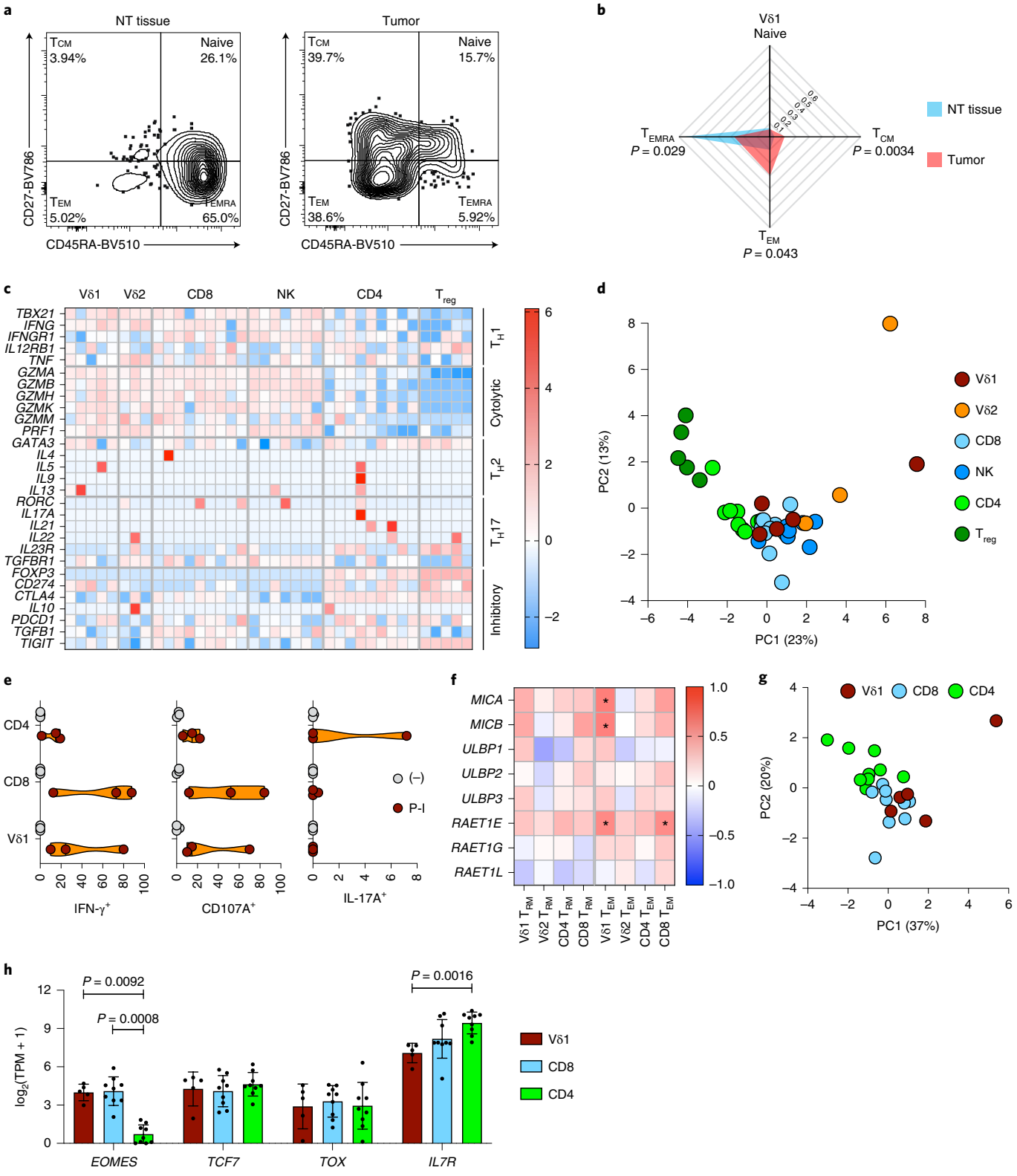

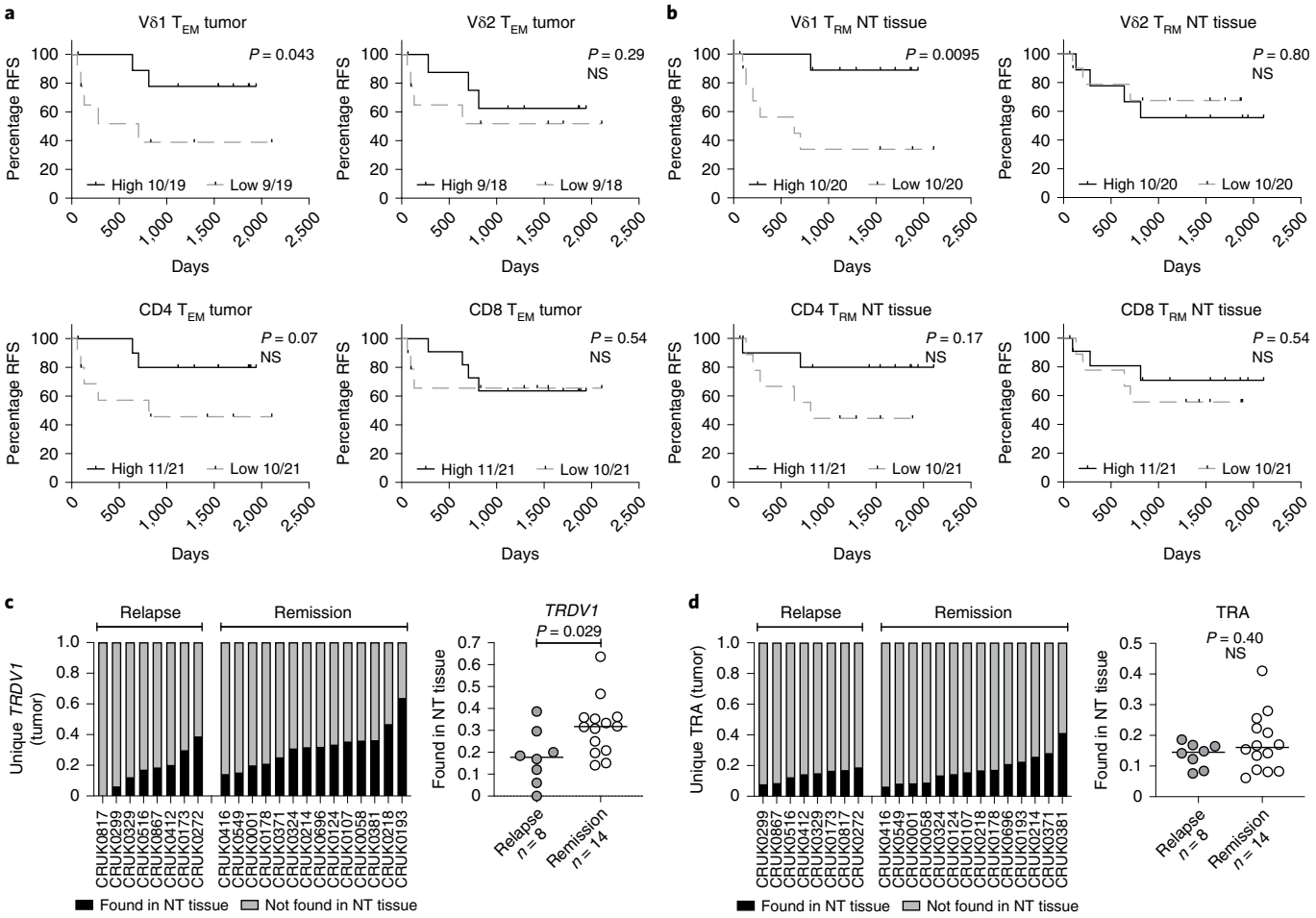

Fig. 4 | Presence of Vd1 T cells associates with RFS in resected NSCLCs. a, RFS split on median absolute numbers of Vδ1, Vδ2, CD4$^+$ and CD8$^+$ T_{EM} cells in tumors. The Gehan–Breslow–Wilcoxon test was used. **b**, RFS split on median absolute numbers of Vδ1, Vδ2, CD4$^+$ and CD8$^+$ T_{RM} cells in NT tissues. The Gehan–Breslow–Wilcoxon test was used. **c**, Proportion of unique Vδ1 (*TRDV1*) T cell clones present in tumors and also found in paired NT tissues. The bar represents the median. A two-tailed Mann–Whitney *U*-test was used. **d**, Proportion of unique αβ (TRA) T cell clones present in tumors and also found in paired NT tissues. The bar represents the median. A two-tailed Mann–Whitney *U*-test was used. Significant *P* values are shown. NS, not significant. The *n* numbers and datapoints represent independent patients.

dichotomous roles of γδ T cells in cancer immunosurveillance and immunotherapy are currently contentious[37]. Similar to αβ T cells, γδ T cells comprise distinct functional subsets. Thus, although absolute γδ T cell deficiency predisposes to cancer in mice, it is now increasingly clear that T_H1-cell-skewed, IFN-γ-producing γδ T cells can be tumor rejecting[59] whereas T_H17-cell-skewed, IL-17-producing γδ T cells may be tumor promoting[18,66,67]. The limited evidence for IL-17 production by human γδ T cells, as opposed to murine γδ T cells, is confined mostly to a subset of peripheral blood-derived Vδ2 T cells[40–42]. By contrast, human Vδ1 T cells have been consistently demonstrated to display a tumor-rejecting Tc1 phenotype when activated in vitro[11,12,65] and now we provide evidence of this in situ within the TME. Consistent with this, we found a significant association of intratumoral T_{EM} Vδ1 T cells with ongoing remission. Although this association was based on outcomes in a modest cohort of patients with early stage, surgically resected NSCLCs, we found a similar association between high *TRDV1* expression, as a proxy for intratumoral Vδ1 T cells, and survival in public TCGA data of ~800 patients with NSCLCs. Moreover, the association of Vδ1 T cells with favorable survival in TCGA was most evident in early-stage disease, alluding to the proposed role of γδ T cells as proximal immune sentinels of epithelial stress[59]. Our study does not directly address their role in metastatic disease where both the tumor-intrinsic biology and immune microenvironment, particularly at disparate metastatic sites, may be different. Likewise, we did not examine other immune compartments, such as the myeloid compartment or tertiary lymphoid structures, which may well contribute and warrant further study. Whether or not Vδ1 T cells directly effect tumor control or are merely a correlate of ongoing remission is difficult to answer without interventional studies such as adoptive Vδ1 T cell therapy, the first of which is currently under way for hematological cancers (NCT05001451). Nevertheless, the association of *TRDV1* expression with favorable responses to CPI therapy alludes to an important role for Vδ1 T cells. Indeed, a recent small study of mismatch repair-deficient colorectal cancers also implicated Vδ1 T cells in positive CPI responses[68].

In considering the utilization of the Vδ1 subset of γδ T cells for cancer immunotherapy, one can now perceive several advantages over Vδ2 T cells. Vδ1 T cells are already resident in steady-state body surface tissues, raising the possibility that these cells may be beneficially manipulated in the clinic by off-the-shelf therapies, for example, via monoclonal antibodies targeting regulatory/stimulatory molecules[69]. Within tumors themselves, Vδ1 T cells display a tissue-resident CD103$^+$ phenotype, potentially improving their tumor-homing and tumor-retention capabilities vis-à-vis adoptive cell therapy. Finally, Vδ1 T cells have been demonstrated by others

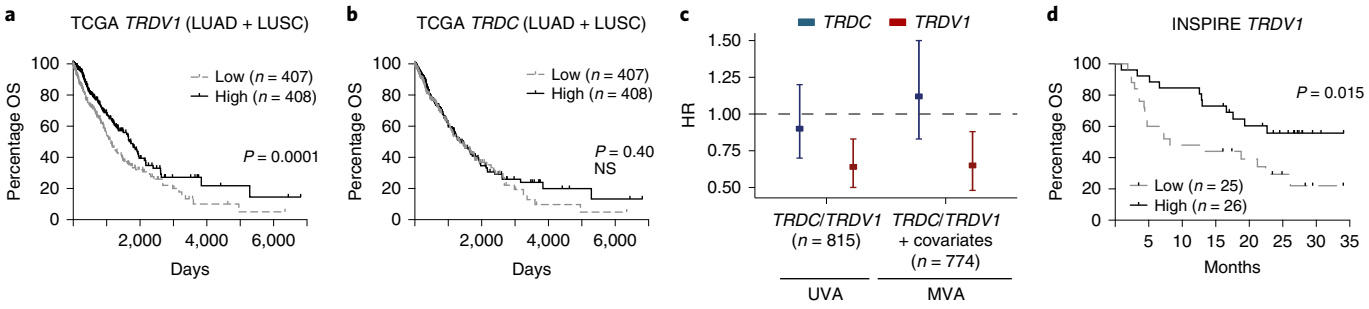

Fig. 5 | Expression of *TRDV1* gene predicts NSCLC survival in TCGA and survival post-pembrolizumab in advanced solid cancers. a, OS of patients with LUAD or LUSC in TCGA split on median *TRDV1* expression in primary tumor as a proxy for intratumoral Vδ1 T cells ($n = 815$ patients). The Gehan–Breslow–Wilcoxon test was used. **b**, OS of the same cohort of patients split on median *TRDC* expression as a proxy for intratumoral γδ T cells ($n = 815$ patients). The Gehan–Breslow–Wilcoxon test was used. NS, not significant. **c**, HRs for death in patients with above-median intratumoral expression of *TRDC* or *TRDV1* in UVA ($n = 815$ patients) and MVA ($n = 774$ patients) with age, gender, histology, smoking status, stage and *CD4* and *CD8B* gene expression. Rounded rectangles denote HRs and error bars denote 95% CIs. **d**, OS of patients with advanced solid cancers (mixed histologies) treated with pembrolizumab in the INSPIRE trial. There was a survival split on median *TRDV1* expression in primary tumor before pembrolizumab. The results were plotted in months after the third cycle of pembrolizumab. The Gehan–Breslow–Wilcoxon test was used. Significant *P* values are shown.

to be less susceptible to activation-induced cell death, a key barrier to durable responses in adoptive cell therapy[70].

Methods

Patients and samples. All clinical samples used were collected from patients recruited to the lung TRACERx Study (approved by an independent Research Ethics Committee, NRES Committee London, REC:13/LO/1546, https://clinicaltrials.gov/ct2/show/NCT01888601). All participants provided informed consent before taking part. Participants were not compensated. Tissue specimens were reviewed by a lung pathologist as previously described[22]. Of note, NT tissues were taken as far away as possible from tumors at primary surgery and H&E sections examined afterwards by a trained histopathologist to ensure samples that were tumor free. Samples were chosen based on the availability of banked TILs from NT lung tissues and paired tumors, region-matched bulk DNA and patients with at least one follow-up visit after surgical resection. Where available, banked contemporaneous PBMCs were also immunophenotyped by flow cytometry. No other selection criteria were applied. Fresh NT tissue and NSCLCs were finely minced with sterile scalpels and dissociated in type 1 collagenase (10 U ml^{-1}, Thermo Fisher Scientific) and DNase I (75 μg ml^{-1}, Roche) on a gentleMACS (Miltenyi Biotech) for 60 min at 37 °C. Digested material was passed through a 0.7-mm cell filter before TIL enrichment by Ficoll-paque gradient centrifugation (GE Healthcare). Isolated TILs were frozen in 10% dimethylsulfoxide (DMSO)/fetal calf serum (FCS) and stored in liquid nitrogen until analysis. PBMCs were isolated from whole blood by Ficoll-paque gradient centrifugation, frozen in FCS with 10% DMSO (v:v) and stored in liquid nitrogen until analysis. DNA from paired tumor regions and paired NT tissues for TCR-seq was extracted as previously described[24]. Briefly, region-matched tissues were homogenized using a TissueRuptor II (QIAGEN) and lysates passed through a QIAshredder column (QIAGEN) before DNA extraction using the Allprep DNA/RNA Mini kit (QIAGEN).

Flow cytometry and FACS. Thawed samples were washed in sterile phosphate-buffered saline (PBS) to remove traces of DMSO and serum before staining with Zombie NIR viability dye (1:500 dilution in PBS for 15 min at room temperature). Samples were then stained for lineage and differentiation markers for 15 min at 4 °C (Supplementary Table 2; all antibodies used at 1:100 dilution in FACS buffer), washed twice with sterile 4 °C FACS buffer, kept on ice and immediately acquired on a BD LSRFortessa or sorted on a BD FACSAria Fusion, running BD FACSDiva, and exported as FCS3.0 files. FCS3.0 files were analyzed on FlowJo v.10. For RNA-seq (see below), cells were sorted directly into ~4 μl of lysis buffer (0.8% Triton X-100 in PBS (v:v) + 2 U ml^{-1} of RNase inhibitor) at 4 °C and lysates frozen at −80 °C. Analysis and results were based on populations with a parent gate of ten or more cells.

In vitro activation assays. Thawed samples were washed in sterile PBS to remove traces of DMSO and rested overnight in complete RPMI medium (10% FCS + penicillin–streptomycin) at 37 °C and 5% CO_2. Rested cells were seeded at up to 200,000 cells per well in 200 μl of complete RPMI medium the next day. Cells either received no stimulation (complete RPMI medium only) or were stimulated with PMA (10 ng ml^{-1}) and ionomycin (1 μg ml^{-1}). Brefeldin A (5 μg ml^{-1}) and anti-CD107A (1:400 final dilution) were added to all the wells. Plates were centrifuged at 200*g* for 2 min and incubated at 37 °C and 5% CO_2 for 5 h. After 5 h, cells were stained for surface lineage markers as described above. After surface staining, samples were fixed in BD CellFIX and washed twice with permeabilization wash buffer (BioLegend) before staining for intracellular cytokines (1:100 final dilution of each antibody in permeabilization wash buffer) for 20 min at 4 °C. Samples were then washed twice with permeabilization wash buffer, resuspended in FACS buffer and immediately acquired on a BD LSRFortessa.

TCR-seq. The gDNA, 3 μg, extracted from region-matched tumors and NT tissues, was submitted for TCRα and TCRδ (TRA and TRD) sequencing with Adaptive Biotechnologies. Reads were aligned and annotated by Adaptive Biotechnologies. Sequences were filtered for in-frame CDR3 cells as well as TRA to TRA V-J family joins for αβ T cells and TRD to TRD V-J family joins for γδ T cells. Absolute counts of TCRs were normalized to 1 μg of input DNA for each sample to enable normalized comparison of T cell numbers across all samples. Data were analyzed using the immunoSEQ ANALYZER v.3.0 (Adaptive Biotechnologies).

RNA-seq of sorted TIL populations, data processing and PCAs. Where sufficient material was available, NK cells and T cell subsets (Vδ1, Vδ2, CD4$^+$, CD8$^+$ and T_{reg} cells) were sorted (50–500 cells from each subset) from NT tissues and tumors from a cohort of donors (patient IDs: CRUK0230, CRUK0299, CRUK0329, CRUK0344, CRUK0412, CRUK0416, CRUK0516, CRUK0860, CRUK0844, CRUK0926, CRUK0949, CRUK0968, CRUK0914, CRUK0961 and CRUK0922). Given the limited availability of material, not all cell types could be sorted from the same samples. Sorted cell lysates were frozen at −80 °C and submitted to the Oxford Genomics Centre for low-input library preparation and sequencing. Library preparation was completed from sorted cells in lysate buffer using the Smart-Seq2 protocol with minor modifications and NexteraXT (Illumina) following the manufacturer's instructions. Libraries were amplified (12 cycles) on a Tetrad (BioRad) using in-house dual indexing primers. Individual libraries were normalized using Qubit and the size profile was analyzed on the TapeStation 4200. Individual libraries were normalized and pooled together accordingly. The pooled library was diluted to ~10 nM for storage. The 10-nM library was denatured and further diluted before loading on the sequencer. Paired-end sequencing was performed using a HiSeq4000 75-bp platform (Illumina, HiSeq 3000/4000 PE Cluster Kit and 150-cycle SBS Kit), generating a raw read count of ~10 million reads per sample. The Trim Galore! utility v.0.4.2 (https://www.bioinformatics.babraham.ac.uk/projects/trim_galore—retrieved 3 May 2017) was used to remove sequencing adapters and quality trim individual reads with the *q*-parameter set to 20. Sequencing reads were aligned to the human genome and transcriptome (Ensembl GRCh38release-89) using RSEM v.1.3.0 (ref. [71]) together with STAR aligner v.2.5.2 (ref. [72]). Sequencing quality of individual samples was assessed using FASTQC v.0.11.5 (https://www.bioinformatics.babraham.ac.uk/projects/fastqc—retrieved 3 May 17) and RNA-SeQC v.1.1.8 (ref. [73]). PCAs were generated using normalized counts of the top 500 variable genes filtered for an average transcripts per million (TPM) across all samples >1 (Extended Data Fig. 3b) or normalized counts of curated master transcription factors and effector molecules presented in Fig. 3c (Fig. 3d).

Region-matched NKG2D ligand gene expression. For each region-matched sample, total RNA was extracted and prepared using a TruSeq Stranded Total RNA Human/Mouse/Rat ribo-depletion library preparation kit before Illumina complementary DNA paired-end sequencing. Libraries were prepared with

≥100 ng of total RNA input where possible and PCR amplified for 15 cycles. Libraries were quality checked by Agilent Tapestation and Promega QuantiFluor double-stranded DNA and pooled in equimolar amounts. Pooled libraries were sequenced in a HiSeq4000 at 50 million raw reads per sample, with a length of 75 bp or 100 bp per read. Illumina adapters were trimmed from raw reads using Cutadapt v.2.10 (ref. [74]) with standard parameters. The quality of the trimmed reads was estimated per flow cell lane using FASTQC v.0.11.9. Fastq files with GC content within 2 s.d. of the cohort mean and <80% of total reads as duplicates were kept for alignment. These were then aligned to the UCSC hg19 human reference genome build using STAR aligner v.2.5.2a[72] in two-pass mode with ENCODE 3 parameters generating one BAM file per tumor region. The same reads were also mapped to the human transcriptome (RefSeq GCA_000001405.1 build) using the same STAR parameters to generate gene expression data. Duplicates were marked with the MarkDuplicates function from GATK v.4.1.7.0 (ref. [75]). Aligned reads were quality checked using QoRTs v.1.3.6 (ref. [76]) for RNA integrity. Somalier v.0.2.7 (ref. [77]) was used to detect potential instances of sample mislabeling. FASTQC, QoRTs and Somalier outputs were visualized using MultiQC v.1.9 (ref. [78]). RSEM v.1.3.3 (ref. [71]) was used with default parameters to quantify gene expression based on the BAM files aligned to the transcriptome. Gene expression patterns were used for further quality control of each sample. Tumor regions with <40% of all genes being expressed (>0 TPM) were excluded. In addition, samples with <20% of reads mapping uniquely to a single location in the genome were excluded.

TCGA analysis. NSCLC data from TCGA were acquired using R software (v.4.0.2). Gene expression data, Workflow Type: HTSeq-Counts and clinical data from the TCGA-LUAD and TCGA-LUSC projects were downloaded from Genomic Data Commons (GDC) Data Portal using the R/Bioconductor package TCGAbiolinks v.2.16.4 (ref. [79]). A total of 594 lung adenocarcinoma (LUAD) and 551 lung squamous cell carcinoma (LUSC) cases were retrieved. Clinical data were utilized to select for primary tumor samples and for patients with OS of at least 1 d, yielding 474 LUAD and 473 LUSC cases. Samples in which *TRDV1* transcript could be detected were included for analysis, thus yielding a final cohort of 417 LUAD and 398 LUSC cases (815 cases in total). Gene expression counts were normalized using DESeq2 v.1.28.1 (ref. [80]) variance stabilizing transformation function and data were filtered for genes of interest: *TRDV1* (Vδ1 T cells) and *TRDC* (γδ cells). For survival analysis, patients were stratified into high- or low-expression groups for each gene of interest using median expression. OS was estimated from clinical data using 'days_to_last_followup' and 'days_to_death' and an OS event was defined from 'vital_status' (Dead/Alive).

The association of *TRDV1* and *TRDC* with survival outcomes in NSCLCs was further assessed by multivariate analysis (MVA) adjusted for age (continuous), gender (categorical), histology (categorical), smoking status (categorical), stage (ordinal), *CD4* expression (above/below median) and *CD8B* expression (above/below median) using the R package Survival (v.3.2-13). Of the variables assessed, only age, gender, histology, *CD4* expression and *CD8B* expression were available for all 815 cases. Smoking status was available for 782 cases and grouped into 'Ex-smokers', 'Current Smokers' and 'Never smokers' using 'tobacco_smoking_history'. Patients with no smoking history information or current reformed smokers with no duration specified were excluded. Stage was available for 806 cases and grouped as stage 1, stage 2 and stage 3/4 owing to very few stage 4 cases. In total, 774 cases (out of 815 for *TRDV1*/*TRDC* univariate analysis (UVA)) were available for MVA.

GTEx analysis. The data used for the analyses described in Extended Data Fig. 2 were obtained from the GTEx portal (www.gtexportal.org/) and GTEx Analysis Release v.8 (dbGaP accession no. phs000424.v8.p2) based on a search for *TRDC*/*TRDV1*/*TRDV2* without any further selection criteria. The data were accessed on 14 January 2022. Detailed methods for the GTEx project are available from the GTEx portal.

Blood atlas analysis. The data used for analysis in Extended Data Fig. 5 were generated as part of the Blood Atlas Study[39]. Gene expression data were downloaded from https://www.proteinatlas.org/about/download on 14 January 2022. TPM values were extracted from 'gdT cell', 'memory CD4 T cell', 'memory CD8 T cell', 'NK-cell' and 'T_{reg}' cell types, $\log_2(TPM+1)$ transformed and z normalized across each gene.

INSPIRE survival analysis. Pre-processed RNA-seq and clinical data were downloaded for 51 patients in the INSPIRE cohort (NCT02644369) for whom both baseline gene expression and OS data were available. This pembrolizumab-treated cohort featured patients with a range of advanced solid cancers: head and neck (head and neck squamous cell cancers, $n=9$), TNBCs ($n=6$), high-grade serous carcinoma ($n=8$), melanoma ($n=8$) and other mixed solid tumors ($n=20$). TPM values that had been $\log_2$(transformed) and batch normalized were downloaded as SourceData_Fig4.zip from Yang et al.[56] and survival split on median expression of each gene.

Statistics and reproducibility. No statistical method was used to predetermine sample size. Samples were chosen based on the availability of materials as described above. Three samples were excluded from outcome analysis due to involved margins on primary resection. The experiments were not randomized and investigators were not blinded to outcomes. The statistical tests used are indicated in the accompanying figure legends and two sided, where applicable, unless otherwise stated. Bonferroni's correction was used to correct for multiple tests. All findings were considered significant at a P-value threshold of 0.05. Significant P values are indicated within the figures. Plots and graphs were generated with GraphPad Prism v.9 and JMP Pro v.15.

Reporting Summary. Further information on research design is available in the Nature Research Reporting Summary linked to this article.

Data availability

The tumor region RNA-seq data, TCR-seq data and flow cytometry data (in each case from the TRACERx study) used or analyzed during the present study are available through the CRUK–University College London Cancer Trials Centre (ctc.tracerx@ucl.ac.uk) for academic noncommercial research purposes only, subject to review of a project proposal that will be evaluated by a TRACERx data access committee and any applicable ethical approvals, and entered into an appropriate data access agreement. Restrictions apply to the data availability to safeguard patient sequence data confidentiality, ensure compliance with patient study consent and meet data protection legislation, and due to commercial partnership requirements.

Details of all public datasets obtained from third parties used in the present study are as follows. Blood Atlas Study (https://doi.org/10.1126/science.aax9198) transcriptomic data were downloaded from https://www.proteinatlas.org/about/download. GTEx (www.gtexportal.org) Analysis Release v.8 was accessed via dbGaP (accession no. phs000424.v8.p2). INSPIRE trial (NCT02644369) transcriptomic data were downloaded as SourceData_Fig4.zip from Yang et al. (https://doi.org/10.1038/s41467-021-25432-7). TCGA human LUAD and LUSC transcriptomic data were downloaded directly using the TCGAbiolinks R package derived from TCGA repository: https://portal.gdc.cancer.gov. Source data are provided with this paper.

Code availability

No customized code was used in the present study.

Received: 26 October 2021; Accepted: 11 April 2022;
Published online: 30 May 2022

References

1. Allen, E. M. V. et al. Genomic correlates of response to CTLA-4 blockade in metastatic melanoma. *Science* **350**, 207–211 (2015).
2. Rizvi, N. A. et al. Mutational landscape determines sensitivity to PD-1 blockade in non-small cell lung cancer. *Science* **348**, 124–128 (2015).
3. McGranahan, N. et al. Clonal neoantigens elicit T cell immunoreactivity and sensitivity to immune checkpoint blockade. *Science* **351**, 1463–1469 (2016).
4. Hellmann, M. D. et al. Nivolumab plus ipilimumab in lung cancer with a high tumor mutational burden. *N. Engl. J. Med.* https://doi.org/10.1056/nejmoa1801946 (2018).
5. Tumeh, P. C. et al. PD-1 blockade induces responses by inhibiting adaptive immune resistance. *Nature* **515**, 568–571 (2014).
6. Sade-Feldman, M. et al. Defining T cell states associated with response to checkpoint immunotherapy in melanoma. *Cell* **175**, 998–1013.e20 (2018).
7. Shim, J. H. et al. HLA-corrected tumor mutation burden and homologous recombination deficiency for the prediction of response to PD-(L)1 blockade in advanced non-small-cell lung cancer patients. *Ann. Oncol.* **31**, 902–911 (2020).
8. Ansell, S. M. et al. PD-1 blockade with nivolumab in relapsed or refractory Hodgkin's lymphoma. *N. Engl. J. Med.* https://doi.org/10.1056/nejmoa1411087 (2014).
9. Hellmann, M. D. et al. Genomic features of response to combination immunotherapy in patients with advanced non-small-cell lung cancer. *Cancer Cell* **33**, e4 (2018).
10. Gentles, A. J. et al. The prognostic landscape of genes and infiltrating immune cells across human cancers. *Nat. Med.* **21**, 938–945 (2015).
11. Wu, Y. et al. An innate-like Vδ1$^+$ γδ T cell compartment in the human breast is associated with remission in triple-negative breast cancer. *Sci. Transl. Med.* **11**, eaax9364 (2019).
12. Mikulak, J. et al. NKp46-expressing human gut-resident intraepithelial Vδ1 T cell subpopulation exhibits high antitumor activity against colorectal cancer. *JCI Insight* **4**, 8900–8920 (2019).
13. Foord, E., Arruda, L. C. M., Gaballa, A., Klynning, C. & Uhlin, M. Characterization of ascites- and tumor-infiltrating γδ T cells reveals distinct repertoires and a beneficial role in ovarian cancer. *Sci. Transl. Med.* **13**, eabb0192 (2021).
14. Zakeri, N. et al. Characterisation and induction of tissue-resident gamma delta T cells to target hepatocellular carcinoma. *Nat. Commun.* **13**, 1372 (2022).

15. Hayday, A. C. & Vantourout, P. The innate biologies of adaptive antigen rReceptors. *Annu. Rev. Immunol.* **38**, 1–24 (2020).
16. Girardi, M. et al. Regulation of cutaneous malignancy by gammadelta T cells. *Science* **294**, 605–609 (2001).
17. Girardi, M. et al. The distinct contributions of murine T cell receptor (TCR) γδ$^+$ and TCRαβ$^+$ T cells to different stages of chemically induced skin cancer. *J. Exp. Med.* **198**, 747–755 (2003).
18. Wu, P. et al. γδT17 cells promote the accumulation and expansion of myeloid-derived suppressor cells in human colorectal cancer. *Immunity* **40**, 785–800 (2014).
19. Daley, D. et al. γδ T cells support pancreatic oncogenesis by restraining αβ T cell activation. *Cell* **166**, 1485–1499.e15 (2016).
20. Carding, S. R. & Egan, P. J. Gammadelta T cells: functional plasticity and heterogeneity. *Nat. Rev. Immunol.* **2**, 336–345 (2002).
21. Craven, K. E., Gökmen-Polar, Y. & Badve, S. S. CIBERSORT analysis of TCGA and METABRIC identifies subgroups with better outcomes in triple negative breast cancer. *Sci. Rep.* **11**, 4691 (2021).
22. Jamal-Hanjani, M. et al. Tracking the evolution of non-small-cell lung cancer. *N. Engl. J. Med.* **376**, 2109–2121 (2017).
23. Zappa, C. & Mousa, S. A. Non-small cell lung cancer: current treatment and future advances. *Transl. Lung Cancer Res.* **5**, 288–300 (2016).
24. Rosenthal, R. et al. Neoantigen-directed immune escape in lung cancer evolution. *Nature* **567**, 479–485 (2019).
25. Alexandrov, L. B. et al. Signatures of mutational processes in human cancer. *Nature* **500**, 415–421 (2013).
26. Shankaran, V. et al. IFNγ and lymphocytes prevent primary tumour development and shape tumour immunogenicity. *Nature* **410**, 1107–1111 (2001).
27. Gao, J. et al. Loss of IFN-γ pathway genes in tumor cells as a mechanism of resistance to anti-CTLA-4 therapy. *Cell* **167**, 397–404.e9 (2016).
28. Rooney, M. S., Shukla, S. A., Wu, C. J., Getz, G. & Hacohen, N. Molecular and genetic properties of tumors associated with local immune cytolytic activity. *Cell* **160**, 48–61 (2015).
29. Pang, D. J., Neves, J. F., Sumaria, N. & Pennington, D. J. Understanding the complexity of γδ T cell subsets in mouse and human. *Immunology* **136**, 283–290 (2012).
30. Carithers, L. J. et al. A novel approach to high-quality postmortem tssue procurement: the GTEx project. *Biopreserv. Biobank* **13**, 311–319 (2015).
31. Farber, D. L., Yudanin, N. A. & Restifo, N. P. Human memory T cells: generation, compartmentalization and homeostasis. *Nat. Rev. Immunol.* **14**, 24–35 (2013).
32. Purwar, R. et al. Resident memory T cells (T_{RM}) are abundant in human lung: diversity, function, and antigen specificity. *PLoS ONE* **6**, e16245 (2011).
33. Snyder, M. E. et al. Generation and persistence of human tissue-resident memory T cells in lung transplantation. *Sci. Immunol.* **4**, eaav5581 (2019).
34. Webb, J. R., Milne, K. & Nelson, B. H. PD-1 and CD103 are widely coexpressed on prognostically favorable intraepithelial CD8 T cells in human ovarian cancer. *Cancer Immunol.* **3**, 926–935 (2015).
35. Savas, P. et al. Single-cell profiling of breast cancer T cells reveals a tissue-resident memory subset associated with improved prognosis. *Nat. Med.* **24**, 986–993 (2018).
36. Djenidi, F. et al. CD8$^+$CD103$^+$ tumor-infiltrating lymphocytes are tumor-specific tissue-resident memory T cells and a prognostic factor for survival in lung cancer patients. *J. Immunol.* **194**, 3475–3486 (2015).
37. Silva-Santos, B., Mensurado, S. & Coffelt, S. B. γδ T cells: pleiotropic immune effectors with therapeutic potential in cancer. *Nat. Rev. Cancer* https://doi.org/10.1038/s41568-019-0153-5 (2019).
38. Davey, M. S. et al. Clonal selection in the human Vδ1 T cell repertoire indicates γδ TCR-dependent adaptive immune surveillance. *Nat. Commun.* **8**, 14760 (2017).
39. Uhlen, M. et al. A genome-wide transcriptomic analysis of protein-coding genes in human blood cells. *Science* **366**, eaax9198 (2019).
40. Ness-Schwickerath, K. J., Jin, C. & Morita, C. T. Cytokine requirements for the differentiation and expansion of IL-17A- and IL-22-producing human Vγ2Vδ2 T cells. *J. Immunol.* **184**, 7268–7280 (2010).
41. Tan, L. et al. A fetal wave of human type 3 effector γδ cells with restricted TCR diversity persists into adulthood. *Sci. Immunol.* **6**, eabf0125 (2021).
42. Caccamo, N. et al. Differentiation, phenotype, and function of interleukin-17–producing human Vγ9Vδ2 T cells. *Blood* **118**, 129–138 (2011).
43. Groh, V., Steinle, A., Bauer, S. & Spies, T. Recognition of stress-induced MHC molecules by intestinal epithelial γδ T cells. *Science* **279**, 1737–1740 (1998).
44. Sherwood, A. M. et al. Deep sequencing of the human TCRγ and TCRβ repertoires suggests that TCRβ rearranges after αβ and γδ T cell commitment. *Sci. Transl. Med.* **3**, 90ra61 (2011).
45. Szabo, P. A., Miron, M. & Farber, D. L. Location, location, location: tissue resident memory T cells in mice and humans. *Sci. Immunol.* **4**, eaas9673 (2019).
46. Bergsbaken, T. & Bevan, M. J. Proinflammatory microenvironments within the intestine regulate differentiation of tissue-resident CD8 T cells responding to infection. *Nat. Immunol.* **16**, 406–414 (2015).
47. Christo, S. N. et al. Discrete tissue microenvironments instruct diversity in resident memory T cell function and plasticity. *Nat. Immunol.* https://doi.org/10.1038/s41590-021-01004-1 (2021).
48. Mackay, L. K. et al. The developmental pathway for CD103$^+$CD8$^+$ tissue-resident memory T cells of skin. *Nat. Immunol.* **14**, 1294–1301 (2013).
49. Kumar, B. V. et al. Human tissue-resident memory T cells are defined by core transcriptional and functional signatures in lymphoid and mucosal sites. *Cell Rep.* **20**, 2921–2934 (2017).
50. Im, S. J. et al. Defining CD8$^+$ T cells that provide the proliferative burst after PD-1 therapy. *Nature* **537**, 417–421 (2016).
51. Alfei, F. et al. TOX reinforces the phenotype and longevity of exhausted T cells in chronic viral infection. *Nature* **571**, 265–269 (2019).
52. Eberhardt, C. S. et al. Functional HPV-specific PD-1$^+$ stem-like CD8 T cells in head and neck cancer. *Nature* **597**, 279–284 (2021).
53. Siddiqui, I. et al. Intratumoral Tcf1$^+$PD-1$^+$CD8$^+$ T cells with stem-like properties promote tumor control in response to vaccination and checkpoint blockade immunotherapy. *Immunity* **50**, 195–211.e10 (2019).
54. McCarthy, N. E. & Eberl, M. Human γδ T cell control of mucosal immunity and inflammation. *Front. Immunol.* **9**, 985 (2018).
55. Villartay, J.-P., de Hockett, R. D., Coran, D., Korsmeyer, S. J. & Cohen, D. I. Deletion of the human T cell receptor δ-gene by a site-specific recombination. *Nature* **335**, 170–174 (1988).
56. Yang, S. Y. C. et al. Pan-cancer analysis of longitudinal metastatic tumors reveals genomic alterations and immune landscape dynamics associated with pembrolizumab sensitivity. *Nat. Commun.* **12**, 5137 (2021).
57. Schenkel, J. M. & Masopust, D. Tissue-resident memory T cells. *Immunity* **41**, 886–897 (2014).
58. Strid, J. et al. Acute upregulation of an NKG2D ligand promotes rapid reorganization of a local immune compartment with pleiotropic effects on carcinogenesis. *Nat. Immunol.* **9**, 146–154 (2008).
59. Gao, Y. et al. γδ T cells provide an early source of interferon γ in tumor immunity. *J. Exp. Med.* **198**, 433–442 (2003).
60. Wu, Y. et al. Human gamma delta T cells: a lymphoid lineage cell capable of professional phagocytosis. *J. Immunol.* **183**, 5622–5629 (2009).
61. Junqueira, C. et al. γδ T cells suppress *Plasmodium falciparum* blood-stage infection by direct killing and phagocytosis. *Nat. Immunol.* https://doi.org/10.1038/s41590-020-00847-4 (2021).
62. Brandes, M., Willimann, K. & Moser, B. Professional antigen-presentation function by human γδ T cells. *Science* **309**, 264–268 (2005).
63. Hayday, A. C. γδ T cell update: adaptate orchestrators of immune surveillance. *J. Immunol.* **203**, 311–320 (2019).
64. Kakimi, K. et al. Adoptive transfer of zoledronate-expanded autologous Vγ9Vδ2 T cells in patients with treatment-refractory non-small-cell lung cancer: a multicenter, open-label, single-arm, phase 2 study. *J. Immunother. Cancer* **8**, e001185 (2020).
65. Almeida, A. R. et al. Delta one T cells for immunotherapy of chronic lymphocytic leukemia: clinical-grade expansion/ differentiation and preclinical proof-of-concept. *Clin. Cancer Res.* **22**, 5795–5804 (2016).
66. Coffelt, S. B. et al. IL-17-producing γδ T cells and neutrophils conspire to promote breast cancer metastasis. *Nature* **522**, 345–348 (2015).
67. Jin, C. et al. Commensal microbiota promote lung cancer development via γδ T cells. *Cell* **176**, 998–1013 (2019).
68. Vries, N. L. de et al. γδ T cells are effectors of immune checkpoint blockade in mismatch repair-deficient colon cancers with antigen presentation defects. Preprint at *bioRxiv* https://doi.org/10.1101/2021.10.14.464229 (2021).
69. Payne, K. K. et al. BTN3A1 governs antitumor responses by coordinating αβ and γδ T cells. *Science* **369**, 942–949 (2020).
70. Godder, K. T. et al. Long term disease-free survival in acute leukemia patients recovering with increased γδ T cells after partially mismatched related donor bone marrow transplantation. *Bone Marrow Transpl.* **39**, 751–757 (2007).
71. Li, B. & Dewey, C. N. RSEM: accurate transcript quantification from RNA-Seq data with or without a reference genome. *BMC Bioinf.* **12**, 323 (2011).
72. Dobin, A. et al. STAR: ultrafast universal RNA-seq aligner. *Bioinformatics* **29**, 15–21 (2013).
73. DeLuca, D. S. et al. RNA-SeQC: RNA-seq metrics for quality control and process optimization. *Bioinformatics* **28**, 1530–1532 (2012).
74. Martin, M. Cutadapt removes adapter sequences from high-throughput sequencing reads. *EMBnet J* **17**, 10–12 (2011).
75. McKenna, A. et al. The Genome Analysis Toolkit: a MapReduce framework for analyzing next-generation DNA sequencing data. *Genome Res.* **20**, 1297–1303 (2010).
76. Hartley, S. W. & Mullikin, J. C. QoRTs: a comprehensive toolset for quality control and data processing of RNA-Seq experiments. *BMC Bioinf.* **16**, 224 (2015).

77. Pedersen, B. S. et al. Somalier: rapid relatedness estimation for cancer and germline studies using efficient genome sketches. *Genome Med.* **12**, 62 (2020).
78. Ewels, P., Magnusson, M., Lundin, S. & Käller, M. MultiQC: summarize analysis results for multiple tools and samples in a single report. *Bioinformatics* **32**, 3047–3048 (2016).
79. Colaprico, A. et al. TCGAbiolinks: an R/Bioconductor package for integrative analysis of TCGA data. *Nucleic Acids Res.* **44**, e71 (2016).
80. Love, M. I., Huber, W. & Anders, S. Moderated estimation of fold change and dispersion for RNA-seq data with DESeq2. *Genome Biol.* **15**, 550 (2014).

Acknowledgements

We thank the Oxford Genomics Centre at the Wellcome Centre for Human Genetics (funded by Wellcome Trust grant no. 203141/Z/16/Z) for the generation and initial processing of the RNA-seq data from sorted TILs. We thank S. Bola for technical support and S. Vanloo for administrative support. The GTEx project was supported by the Common Fund of the Office of the Director of the National Institutes of Health, and by the NCI, NHGRI, NHLBI, NIDA, NIMH and NINDS. Y.W. was supported by a Wellcome Trust Clinical Research Career Development Fellowship (no. 220589/Z/20/Z), an Academy of Medical Sciences Starter Grant for Clinical Lecturers, a National Institute for Health Research (NIHR) Academic Clinical Lectureship and the NIHR University College London Hospitals Biomedical Research Centre. D.B. was supported by funding from the NIHR University College London Hospitals Biomedical Research Centre, the ideas 2 innovation translation scheme at the Francis Crick Institute, the Breast Cancer Research Foundation (BCRF) and a Cancer Research UK (CRUK) Early Detection and Diagnosis Project award. M.J.H. is a CRUK Fellow and has received funding from CRUK, NIHR, Rosetrees Trust, UKI NETs and the NIHR University College London Hospitals Biomedical Research Centre. C.S. is Royal Society Napier Research Professor. This work was supported by the Francis Crick Institute which receives its core funding from CRUK (no. FC001169), the UK Medical Research Council (no. FC001169) and the Wellcome Trust (no. FC001169). This research was funded in whole, or in part, by the Wellcome Trust (no. FC001169). For the purpose of Open Access, the author has applied a CC BY public copyright license to any Author Accepted Manuscript version arising from this submission. C.S. is funded by CRUK (TRACERx, PEACE and CRUK Cancer Immunotherapy Catalyst Network), CRUK Lung Cancer Centre of Excellence (no. C11496/A30025), the Rosetrees Trust, Butterfield and Stoneygate Trusts, NovoNordisk Foundation (ID16584), Royal Society Professorship Enhancement Award (no. RP/EA/180007), the NIHR Biomedical Research Centre at University College London Hospitals, the CRUK–University College London Centre, Experimental Cancer Medicine Centre and the BCRF. This work was supported by a Stand Up To Cancer-LUNGevity-American Lung Association Lung Cancer Interception Dream Team Translational Research Grant (grant no. SU2C-AACR-DT23-17 to S. M. Dubinett and A. E. Spira). Stand Up To Cancer is a division of the Entertainment Industry Foundation. Research grants are administered by the American Association for Cancer Research, the Scientific Partner of SU2C. C.S. receives funding from the European Research Council (ERC) under the European Union's Seventh Framework Programme (no. FP7/2007-2013) Consolidator Grant (no. FP7-THESEUS-617844), European Commission ITN (no. FP7-PloidyNet 607722), an ERC Advanced Grant (PROTEUS) from the ERC under the European Union's Horizon 2020 research and innovation program (grant no. 835297), and Chromavision from the European Union's Horizon 2020 research and innovation program (grant no. 665233).

Author contributions

Y.W. and D.B. designed and undertook laboratory experiments. Y.W., D.B., I.U., M.A., S.B., C.M., M.J., N.M. and A.H. designed, carried out and/or interpreted bioinformatics analyses and/or experimental data. T.K., S.V., J.C-K, S.H., J.R., A.G., M.A.-B., M.J.-H. and the TRACERx Consortium coordinated the clinical trial, and provided patient samples and patient data. Y.W., D.B., A.C.H. and C.S. wrote the manuscript. Y.W., S.A.Q., A.C.H and C.S. supervised the project. Y.W., A.C.H. and C.S. conceived and designed the project.

Competing interests

D.B. has consulted for NanoString, reports honoraria from AstraZeneca and has a patent (PCT/GB2020/050221) issued on methods for cancer prognostication. J.R. and M.A.B. have consulted for Achilles Therapeutics. N.M. has stock options in and has consulted for Achilles Therapeutics. N.M. holds European patents relating to targeting neoantigens (PCT/EP2016/059401), identifying patient response to immune checkpoint blockade (PCT/EP2016/071471), determining HLA loss of heterozygosity (PCT/GB2018/052004) and predicting survival rates of patients with cancer (PCT/GB2020/050221). A.H. attended one advisory board for Abbvie, Roche and GRAIL, and reports personal fees from Abbvie, Boehringer Ingelheim, Takeda, AstraZeneca, Daiichi Sankyo, Merck Serono, Merck/MSD, UCB and Roche for delivering general education/training in clinical trials. A.H. owned shares in Illumina and Thermo Fisher Scientific (sold in 2020) and receives fees for membership of Independent Data Monitoring Committees for Roche-sponsored clinical trials. S.A.Q. is co-founder and Chief Scientific Officer of Achilles Therapeutics. A.C.H. is a board member and equity holder in ImmunoQure, AG and Gamma Delta Therapeutics, and is an equity holder in Adaptate Biotherapeutics and chair of the scientific advisory board. C.S. acknowledges grant support from Pfizer, AstraZeneca, Bristol Myers Squibb, Roche-Ventana, Boehringer Ingelheim, Archer Dx Inc (collaboration in minimal residual disease-sequencing technologies) and Ono Pharmaceuticals, is an AstraZeneca Advisory Board member and Chief Investigator for the MeRmaiD1 clinical trial. C.S has consulted for Amgen, AstraZeneca, Bicycle Therapeutics, Bristol Myers Squibb, Celgene, Genentech, GlaxoSmithKline, GRAIL, Illumina, Medixci, Metabomed, MSD, Novartis, Pfizer, Roche-Ventana and Sarah Cannon Research Institute. C.S. has stock options in Apogen Biotechnologies, Epic Biosciences and GRAIL, and has stock options and is co-founder of Achilles Therapeutics. C.S. holds patents relating: to assay technology to detect tumor recurrence (PCT/GB2017/053289); to targeting neoantigens (PCT/EP2016/059401), identifying patient response to immune checkpoint blockade (PCT/EP2016/071471), determining HLA loss of heterozygosity (PCT/GB2018/052004), predicting survival rates of patients with cancer (PCT/GB2020/050221); to treating cancer by targeting Insertion/deletion (indel) mutations (PCT/GB2018/051893); to identifying indel mutation targets (PCT/GB2018/051892); to methods for lung cancer detection (PCT/US2017/028013); and to identifying responders to cancer treatment (PCT/GB2018/051912). The remaining authors declare no competing interests.

Additional information

Extended data Extended data are available for this paper at https://doi.org/10.1038/s43018-022-00376-z.

Supplementary information The online version contains supplementary material available at https://doi.org/10.1038/s43018-022-00376-z.

Correspondence and requests for materials should be addressed to Yin Wu, Adrian C. Hayday or Charles Swanton.

Peer review information *Nature Cancer* thanks Jose Conejo-Garcia, Jianjun Zhang and the other, anonymous, reviewer(s) for their contribution to the peer review of this work.

Reprints and permissions information is available at www.nature.com/reprints.

Publisher's note Springer Nature remains neutral with regard to jurisdictional claims in published maps and institutional affiliations.

TRACERx Consortium

Charles Swanton[1,2], Mariam Jamal-Hanjani[1,7], Nicholas McGranahan[1,9], Allan Hackshaw[10], Yin Wu[1,2,3,4,55], Dhruva Biswas[1,2,5,55], Mihaela Angelova[2], Stefan Boeing[6], Takahiro Karasaki[1,2], Selvaraju Veeriah[1], Sonya Hessey[1,7], James Reading[1,8], Maise Al-Bakir[2], Sergio A. Quezada[1,8], Nicolai J. Birkbak[11], Gillian Price[12], Mohammed Khalil[12], Keith Kerr[12], Shirley Richardson[12], Heather Cheyne[12], Tracey Cruickshank[12], Gareth A. Wilson[13], Rachel Rosenthal[13], Hugo Aerts[14,15], Madeleine Hewish[16], Girija Anand[17], Sajid Khan[17], Kelvin Lau[18], Michael Sheaff[18], Peter Schmid[18], Louise Lim[18], John Conibear[18], Roland Schwarz[19], Tom L. Kaufmann[19], Matthew Huska[19], Jacqui Shaw[20],

Joan Riley[20], Lindsay Primrose[20], Dean Fennell[20,21], Allan Hackshaw[22], Yenting Ngai[22], Abigail Sharp[22], Oliver Pressey[22], Sean Smith[22], Nicole Gower[22], Harjot Kaur Dhanda[22], Kitty Chan[22], Sonal Chakraborty[22], Kevin Litchfield[1], Krupa Thakkar[1], Jonathan Tugwood[23], Alexandra Clipson[23], Caroline Dive[23,24], Dominic Rothwell[23,24], Alastair Kerr[23,24], Elaine Kilgour[23,24], Fiona Morgan[25], Malgorzata Kornaszewska[25], Richard Attanoos[25], Helen Davies[25], Katie Baker[26], Mathew Carter[26], Colin R. Lindsay[26], Fabio Gomes[26], Fiona Blackhall[24,26], Lynsey Priest[24,26], Matthew G. Krebs[24,26], Anshuman Chaturvedi[24,26], Pedro Oliveira[24,26], Zoltan Szallasi[27], Gary Royle[28], Catarina Veiga[28], Marcin Skrzypski[29], Roberto Salgado[30], Miklos Diossy[31], Alan Kirk[32], Mo Asif[32], John Butler[32], Rocco Bilancia[32], Nikos Kostoulas[32], Mathew Thomas[32], Mairead MacKenzie[33], Maggie Wilcox[33], Apostolos Nakas[21], Sridhar Rathinam[21], Rebecca Boyles[21], Mohamad Tufail[21], Amrita Bajaj[21], Keng Ang[21], Mohammed Fiyaz Chowdhry[21], Michael Shackcloth[34], Julius Asante-Siaw[34], Angela Leek[35], Nicola Totten[35], Jack Davies Hodgkinson[35], Peter Van Loo[36], William Monteiro[37], Hilary Marshal[37], Kevin G. Blyth[38], Craig Dick[38], Charles Fekete[15], Eric Lim[39], Paulo De Sousa[39], Simon Jordan[39], Alexandra Rice[39], Hilgardt Raubenheimer[39], Harshil Bhayani[39], Morag Hamilton[39], Lyn Ambrose[39], Anand Devaraj[39], Hemangi Chavan[39], Sofina Begum[39], Silviu I. Buderi[39], Daniel Kaniu[39], Mpho Malima[39], Sarah Booth[39], Andrew G. Nicholson[39], Nadia Fernandes[39], Pratibha Shah[39], Chiara Proli[39], John Gosney[40], Sarah Danson[41], Jonathan Bury[41], John Edwards[41], Jennifer Hill[41], Sue Matthews[41], Yota Kitsanta[41], Jagan Rao[41], Sara Tenconi[41], Laura Socci[41], Kim Suvarna[41], Faith Kibutu[41], Patricia Fisher[41], Robin Young[41], Joann Barker[41], Fiona Taylor[41], Kirsty Lloyd[41], Jason Lester[42], Mickael Escudero[43], Aengus Stewart[43], Andrew Rowan[43], Jacki Goldman[43], Richard Kevin Stone[43], Tamara Denner[43], Emma Nye[43], Maria Greco[43], Jerome Nicod[43], Clare Puttick[43], Katey Enfield[43], Emma Colliver[43], Alastair Magness[43], Chris Bailey[43], Krijn Dijkstra[43], Vittorio Barbè[43], Roberto Vendramin[43], Judit Kisistok[43], Mateo Sokac[43], Jonas Demeulemeester[43], Elizabeth Larose Cadieux[43], Carla Castignani[43], Hongchang Fu[43], Kristiana Grigoriadis[43], Claudia Lee[43,44], Foteini Athanasopoulou[1,43], Crispin Hiley[1,43], Lily Robinson[45], Tracey Horey[45], Peter Russell[45], Dionysis Papadatos-Pastos[45], Sara Lock[46], Kayleigh Gilbert[46], Kayalvizhi Selvaraju[47], Paul Ashford[47], Oriol Pich[47], Thomas B. K. Watkins[47], Sophia Ward[47], Emilia Lim[47], Alexander M. Frankell[47], Christopher Abbosh[47], Robert E. Hynds[47], Mariana Werner Sunderland[47], Karl Peggs[47], Teresa Marafioti[47], John A. Hartley[47], Helen Lowe[47], Leah Ensell[47], Victoria Spanswick[47], Angeliki Karamani[47], David Moore[47], Stephan Beck[47], Olga Chervova[47], Miljana Tanic[47], Ariana Huebner[47], Michelle Dietzen[47], James R. M. Black[47], Carlos Martinez Ruiz[47], Robert Bentham[47], Cristina Naceur-Lombardelli[47], Haoran Zhai[47], Nnennaya Kanu[47], Francisco Gimeno-Valiente[47], Supreet Kaur Bola[47], Ignacio Garcia Matos[47], Mansi Shah[47], Felipe Galvez Cancino[47], Despoina Karagianni[47], Maryam Razaq[47], Mita Akther[47], Diana Johnson[47], Joanne Laycock[47], Elena Hoxha[47], Benny Chain[47], David R. Pearce[47], Kezhong Chen[47], Javier Herrero[47], Fleur Monk[47], Simone Zaccaria[47], Neil Magno[47], Paulina Prymas[47], Antonia Toncheva[47], Monica Sivakumar[47], Olivia Lucas[47,48], Mark S. Hill[43,47], Othman Al-Sawaf[47], Seng Kuong Ung[48], Sam Gamble[48], Sophia Wong[48], David Lawrence[48], Martin Hayward[48], Nikolaos Panagiotopoulos[48], Robert George[48], Davide Patrini[48], Mary Falzon[48], Elaine Borg[48], Reena Khiroya[48], Asia Ahmed[48], Magali Taylor[48], Junaid Choudhary[48], Sam M. Janes[48], Martin Forster[48], Tanya Ahmad[48], Siow Ming Lee[48], Neal Navani[48], Marco Scarci[48], Pat Gorman[48], Elisa Bertoja[48], Robert C. M. Stephens[48], Emilie Martinoni Hoogenboom[48], James W. Holding[48], Steve Bandula[48], Ricky Thakrar[48], James Wilson[48], Mansi Shah[48], Marcos[48], Vasquez Duran[48], Maria Litovchenko[48], Sharon Vanloo[48],

Piotr Pawlik[48], Kerstin Thol[48], Babu Naidu[49], Gerald Langman[49], Hollie Bancroft[49], Salma Kadiri[49], Gary Middleton[49], Madava Djearaman[49], Aya Osman[49], Helen Shackleford[49], Akshay Patel[49], Christian Ottensmeier[50], Serena Chee[50], Aiman Alzetani[50], Judith Cave[50], Lydia Scarlett[50], Jennifer Richards[50], Papawadee Ingram[50], Emily Shaw[50], John Le Quesne[51], Alan Dawson[52], Domenic Marrone[52], Sean Dulloo[52], Claire Wilson[52], Yvonne Summers[53], Raffaele Califano[53], Rajesh Shah[53], Piotr Krysiak[53], Kendadai Rammohan[53], Eustace Fontaine[53], Richard Booton[53], Matthew Evison[53], Stuart Moss[53], Juliette Novasio[53], Leena Joseph[53], Paul Bishop[53], Helen Doran[53], Felice Granato[53], Vijay Joshi[53], Elaine Smith[53], Angeles Montero[53] and Phil Crosbie[53,54]

[11]Aarhus University, Aarhus, Denmark. [12]Aberdeen Royal Infirmary, Aberdeen, UK. [13]Achilles Therapeutics UK Limited, London, UK. [14]Artificial Intelligence in Medicine Program, Harvard Medical School, Boston, MA, USA. [15]Radiology and Nuclear Medicine, CARIM & GROW, Maastricht University, Maastricht, The Netherlands. [16]Ashford and St. Peter's Hospitals NHS Foundation Trust, Chertsey, UK. [17]Barnet & Chase Farm Hospitals, London, UK. [18]Barts Health NHS Trust, London, UK. [19]Berlin Institute for Medical Systems Biology, Max Delbrück Center for Molecular Medicine in the Helmholtz Association, Berlin, Germany. [20]Cancer Research Centre, University of Leicester, Leicester, UK. [21]Leicester University Hospitals, Leicester, UK. [22]Cancer Research UK & UCL Cancer Trials Centre, London, UK. [23]Cancer Research UK Manchester Institute, University of Manchester, Manchester, UK. [24]Cancer Research UK Lung Cancer Centre of Excellence, University of Manchester, Manchester, UK. [25]Cardiff & Vale University Health Board, Cardiff, UK. [26]Christie NHS Foundation Trust, Manchester, UK. [27]Danish Cancer Society Research Centre, Copenhagen, Denmark. [28]Department of Medical Physics and Bioengineering, University College London Cancer Institute, London, UK. [29]Department of Oncology and Radiotherapy, Medical University of Gdańsk, Gdańsk, Poland. [30]Department of Pathology, GZA-ZNA Antwerp, Antwerp, Belgium. [31]Department of Physics of Complex Systems, ELTE Eötvös Loránd University, Budapest, Hungary. [32]Golden Jubilee National Hospital, Clydebank, UK. [33]Independent Cancer Patients Voice, London, UK. [34]Liverpool Heart and Chest Hospital NHS Foundation Trust, Liverpool, UK. [35]Manchester Cancer Research Centre Biobank, Manchester, UK. [36]MD Anderson Cancer Center, Houston, TX, USA. [37]National Institute for Health Research, Leicester Respiratory Biomedical Research Unit, Leicester, UK. [38]NHS Greater Glasgow and Clyde, Glasgow, UK. [39]Royal Brompton and Harefield NHS Foundation Trust, London, UK. [40]Royal Liverpool University Hospital, Liverpool, UK. [41]Sheffield Teaching Hospitals NHS Foundation Trust, Sheffield, UK. [42]Swansea Bay University Health Board, Swansea, UK. [43]The Francis Crick Institute, London, UK. [44]University College London Medical School, London, UK. [45]The Princess Alexandra Hospital NHS Trust, Harlow, UK. [46]The Whittington Hospital NHS Trust, London, UK. [47]University College London Cancer Institute, London, UK. [48]University College London Hospitals, London, UK. [49]University Hospital Birmingham NHS Foundation Trust, Birmingham, UK. [50]University Hospital Southampton NHS Foundation Trust, Southampton, UK. [51]Institute of Cancer Sciences, University of Glasgow, Glasgow, UK. [52]University of Leicester, Leicester, UK. [53]Wythenshawe Hospital, Manchester University NHS Foundation Trust, Manchester, UK. [54]Division of Infection, Immunity and Respiratory Medicine, University of Manchester, Manchester, UK.

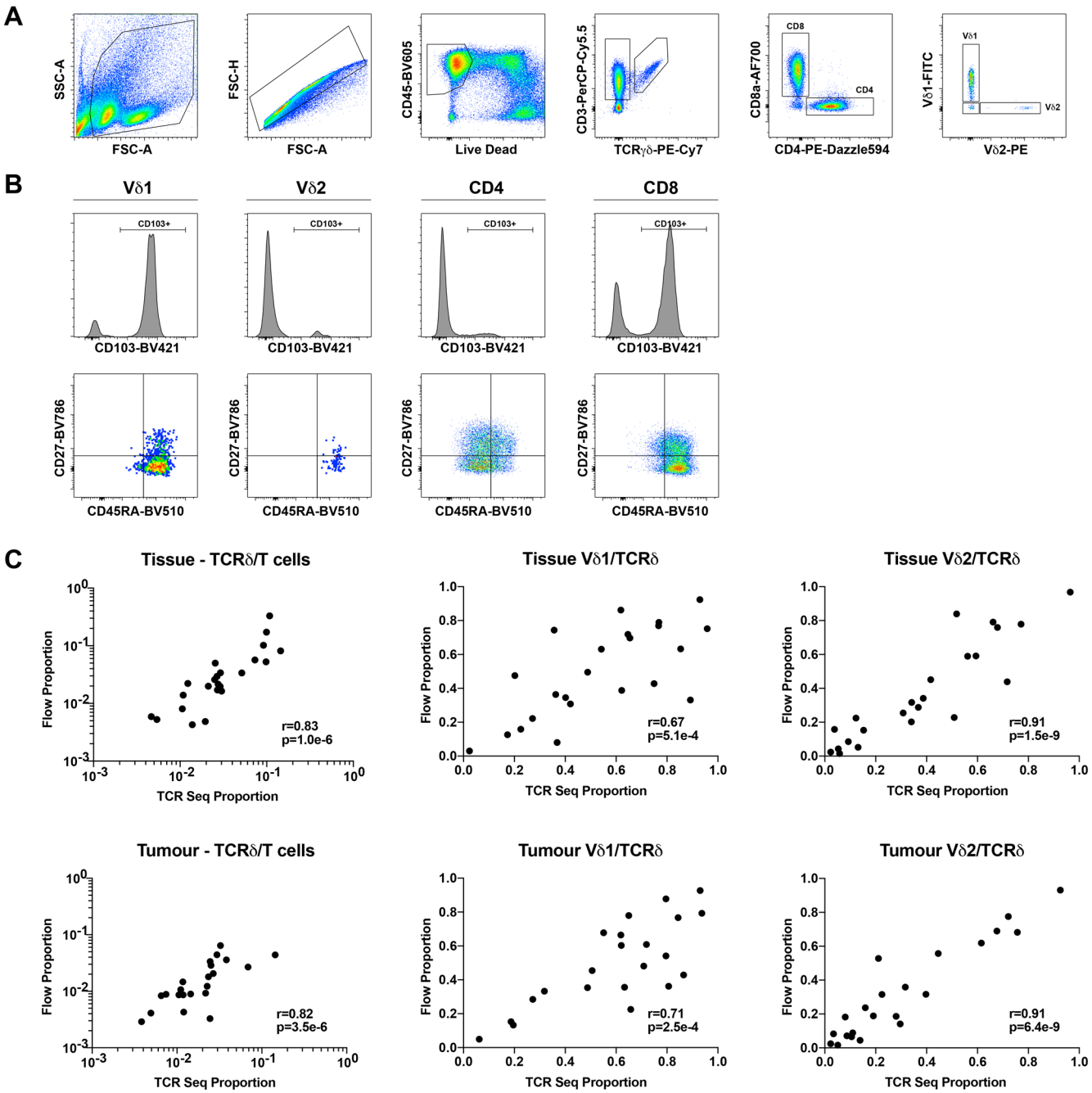

Extended Data Fig. 1 | Lung γδ T cells assayed by flow cytometry and TCR sequencing. A) Representative flow cytometry gating strategy for T cell subsets. From left to right: Forward vs. side scatter gate -> singlet gate -> live CD45 + gate -> CD3 vs. TCRγδ -> CD4 vs. CD8 (of CD3 + /TCRγδ- population) and Vδ1 vs. Vδ2 (of CD3 + / TCRγδ + population) to give CD4 and CD8 αβ T cells and Vδ1 and Vδ2 γδ T cells. **B)** Representative gating strategy for CD103 and CD45RA vs. CD27 for Vδ1 and Vδ2 γδ T cells, and CD4 and CD8 αβ T cells. **C)** Proportion of T cell subsets determined by flow cytometry versus proportion determined by TCRseq in NT tissues (n = 23 patients) and tumours (n = 22 patients). Two-tailed Spearman correlation. Significant p values shown. All datapoints represent independent patients.

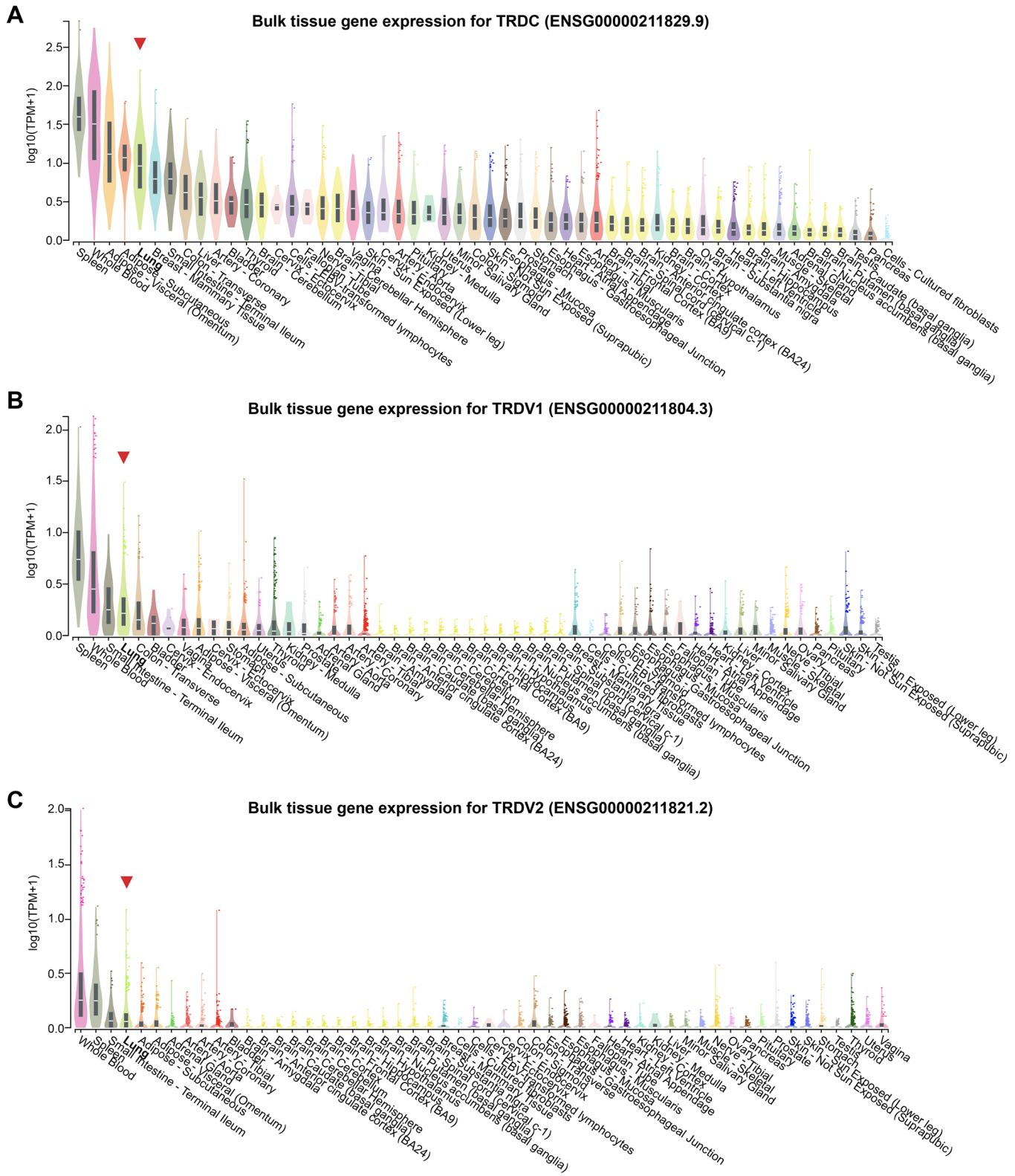

Extended Data Fig. 2 | TCRδ is expressed in non-diseased lung tissues. A) Expression of *TRDC* across non-diseased tissue types. **B)** Expression of *TRDV1* across non-diseased tissue types. **C)** Expression of *TRDV2* across non-diseased tissue types. Gene expression data and figures derived from the GTEx Project and Portal (see methods). Lung expression (red arrow) based on 578 donors. Boxplots represent median and interquartile range with outliers (above or below 1.5x IQR) displayed as points. Tissues ordered from highest to lowest median expression of each gene. Datapoints represent independent donors.

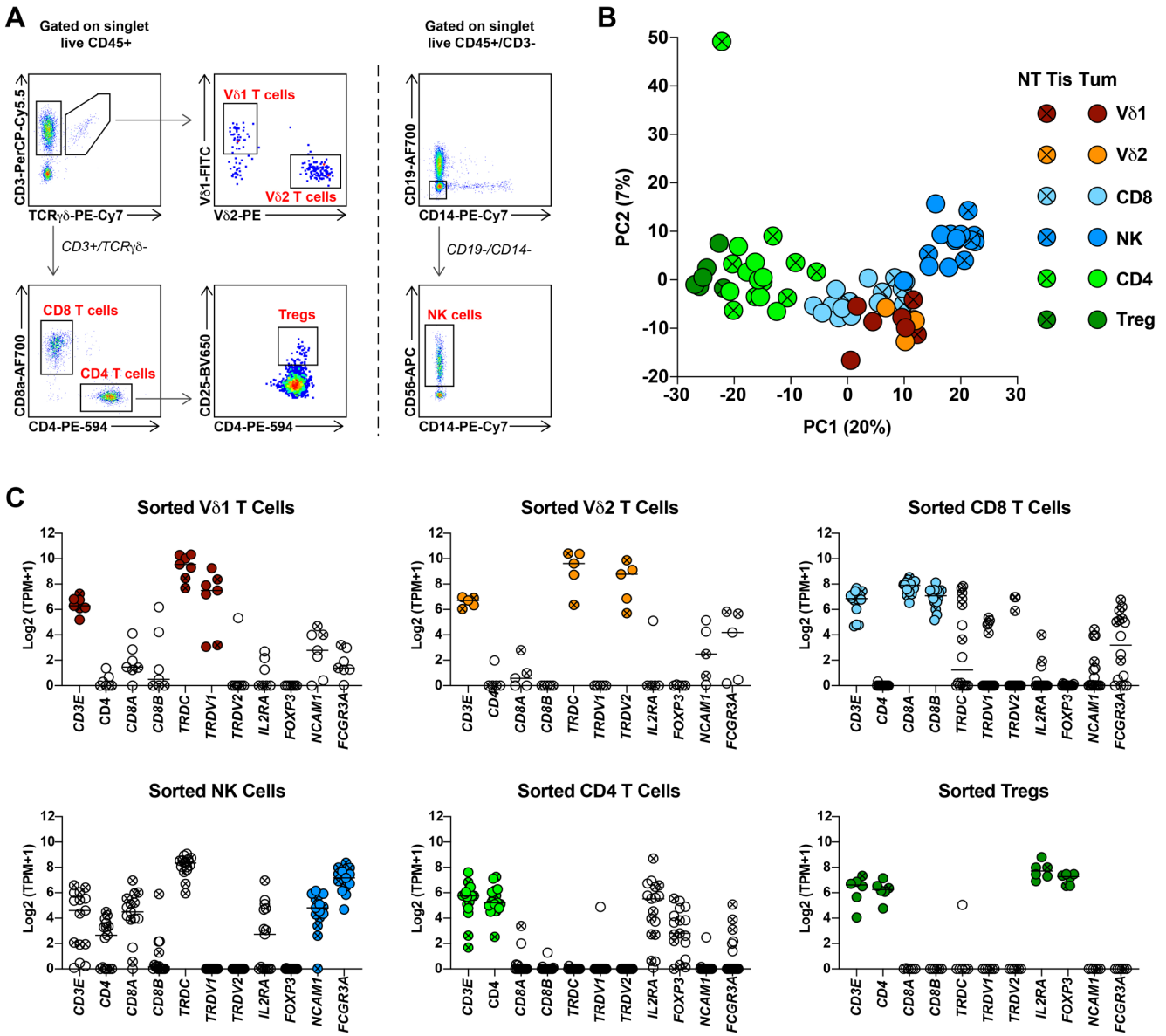

Extended Data Fig. 3 | Lung TIL lineages by RNA sequencing. A) Gating strategy for sorting CD4, CD8, Vδ1 and Vδ2 T cells and Tregs and NK cells (red/bold) for bulk cell-type RNA sequencing. **B)** PCA of top 500 variable genes coloured by cell type from tumours (n = 9, n = 9, n = 7, n = 5, n = 3 and n = 5 patients for CD4+, CD8+, NK, Treg, Vδ2 and Vδ1 cells respectively) and NT tissue (n = 8, n = 7, n = 8, n = 1, n = 2 and n = 2 patients for CD4+, CD8+, NK, Treg, Vδ2 and Vδ1 cells respectively). **C)** Expression of canonical lineage markers from sorted cell types. Lineage markers for each sorted cell type coloured in. Cells sorted from NT tissues denoted by crossed-circles (n = 8, n = 7, n = 8, n = 1, n = 2 and n = 2 patients for CD4+, CD8+, NK, Treg, Vδ2 and Vδ1 cells respectively) and cells sorted from lung tumours denoted by solid circles (n = 9, n = 9, n = 7, n = 5, n = 3 and n = 5 patients for CD4+, CD8+, NK, Treg, Vδ2 and Vδ1 cells respectively). All datapoints represent independent patients.

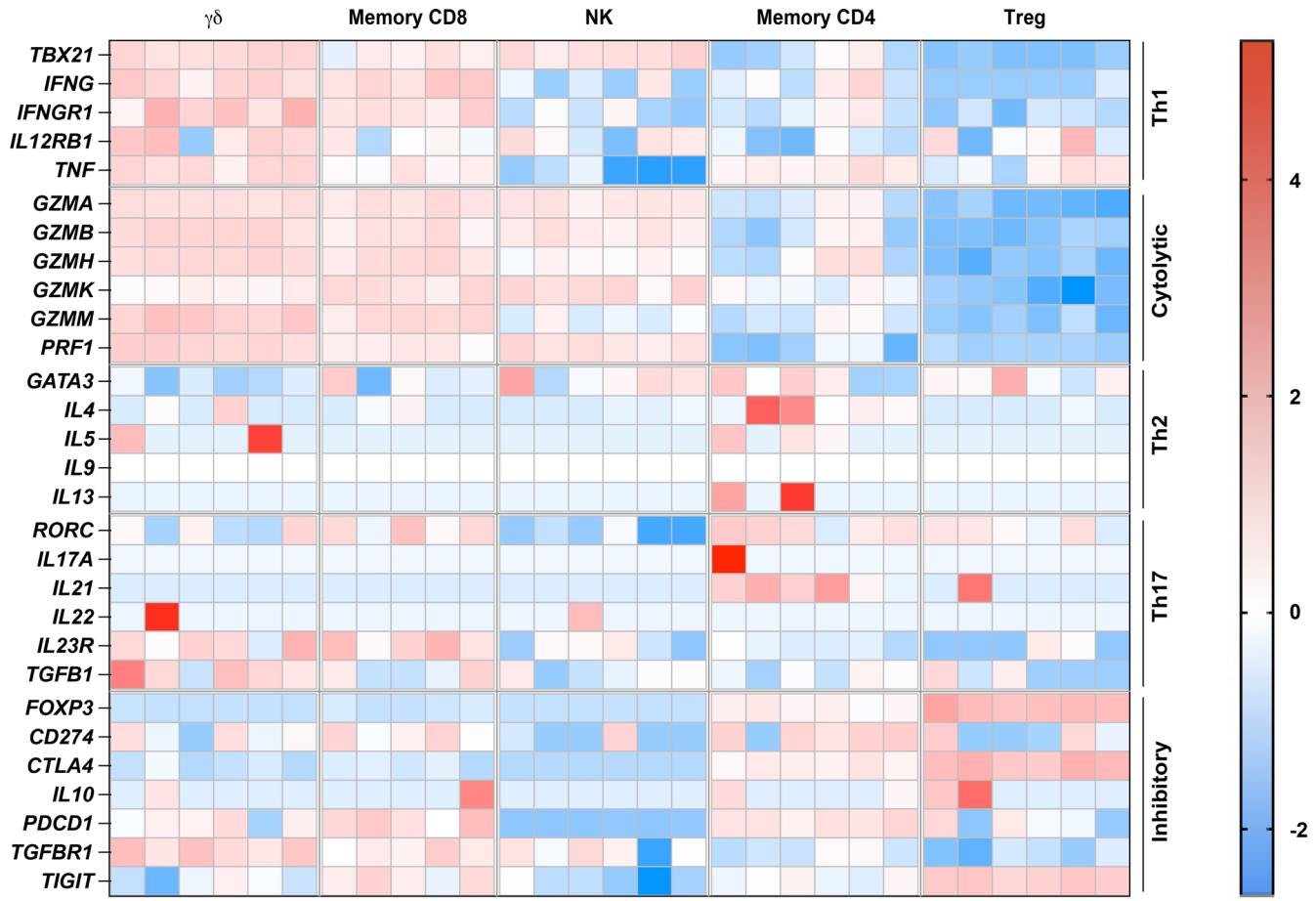

Extended Data Fig. 4 | Peripheral blood γδ T cell functional transcriptomes. Expression of T cell master transcription factors and signature effector molecules of peripheral blood lymphocytes from the Blood Atlas project. Each column represents the denoted cell type from an individual donor. Colour scale denotes Z-score of Log2 (TPM + 1) of each gene.

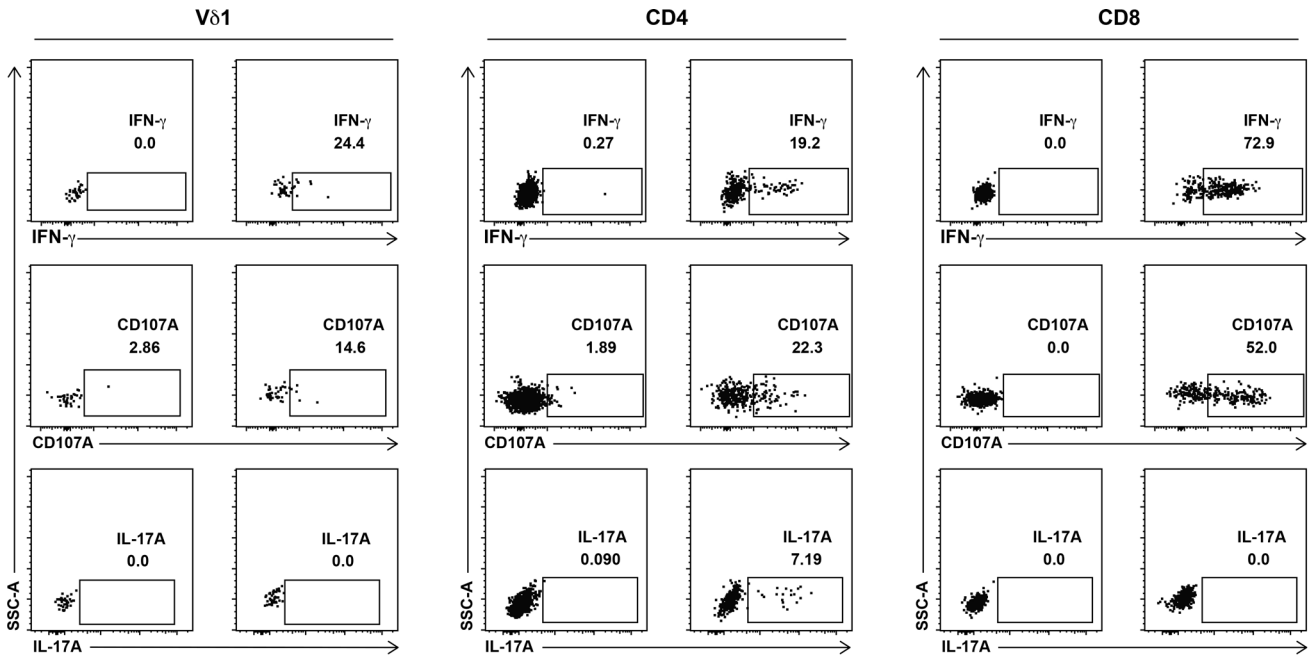

Extended Data Fig. 5 | Effector function of *in vitro* stimulated TILs from NSCLCs. Representative flow cytometry dot plots of intracellular cytokine staining for IFN-γ and IL-17A and cell surface staining for CD107A in Vδ1, CD8 and CD4 T cells after *in vitro* stimulation of bulk tumour infiltrating lymphocytes with PMA and ionomycin (P-I). Gates were set on paired unstimulated negative controls (-). Percentage positive of parent population shown.

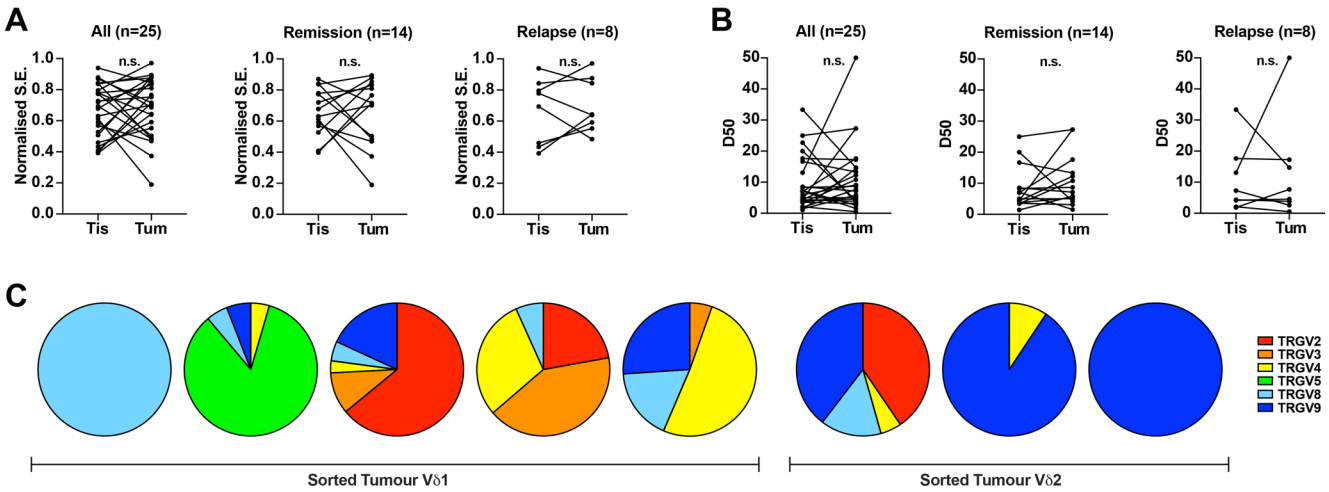

Extended Data Fig. 6 | Tumour Vδ1 T cells demonstrate no evidence of clonotypic responses. A) Repertoire analysis by normalised Shannon entropy (S.E.) of Vδ1 T cells in NT tissue (Tis) and paired lung tumours (Tum) calculated on TCRδ CDR3 amino-acid sequences. Wilcoxon matched-pairs signed rank test. **B)** Repertoire analysis by D50 of Vδ1 T cells in NT tissue (Tis) and paired lung tumours (Tum) calculated on TCRδ CDR3 amino-acid sequences. Wilcoxon matched-pairs signed rank test. **C)** Relative expression (TPM) of functional TCRγ Vγ genes in sorted intra- tumoural Vδ1 T cells from 5 patients and Vδ2 from 3 patients. All datapoints represent independent patients.

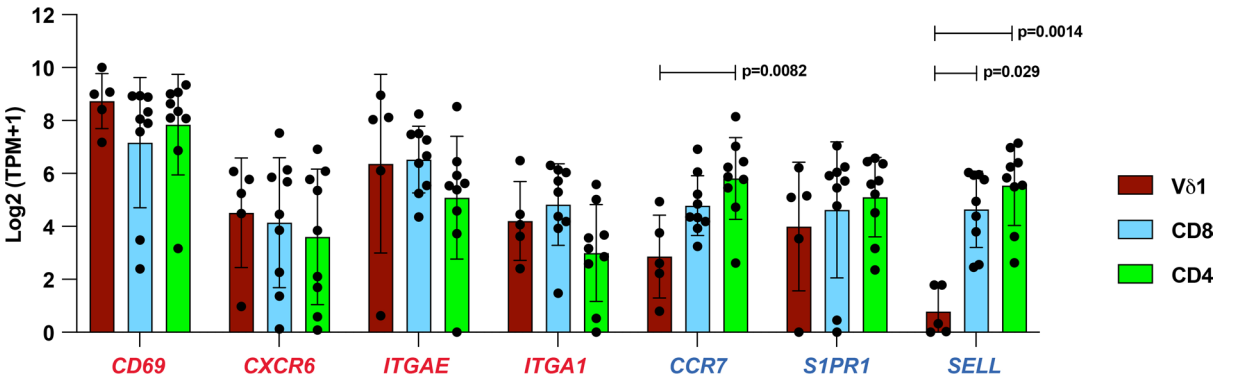

Extended Data Fig. 7 | Tumour Vδ1 T cells possess a core T_{RM} signature. Expression of core TRM signature genes in Vδ1, CD8, and CD4 T cells sorted from tumours (n = 5, n = 9 and n = 9 patients respectively). Genes associated with tissue retention and homing and expected to be upregulated in TRM T cells highlighted in red. Genes associated with tissue egress and expected to be downregulated in TRM T cells highlighted in blue. Mean +/- S.D. plotted. Kruskal Wallis with post hoc Dunn's test corrected for multiple testing. All datapoints represent independent patients.

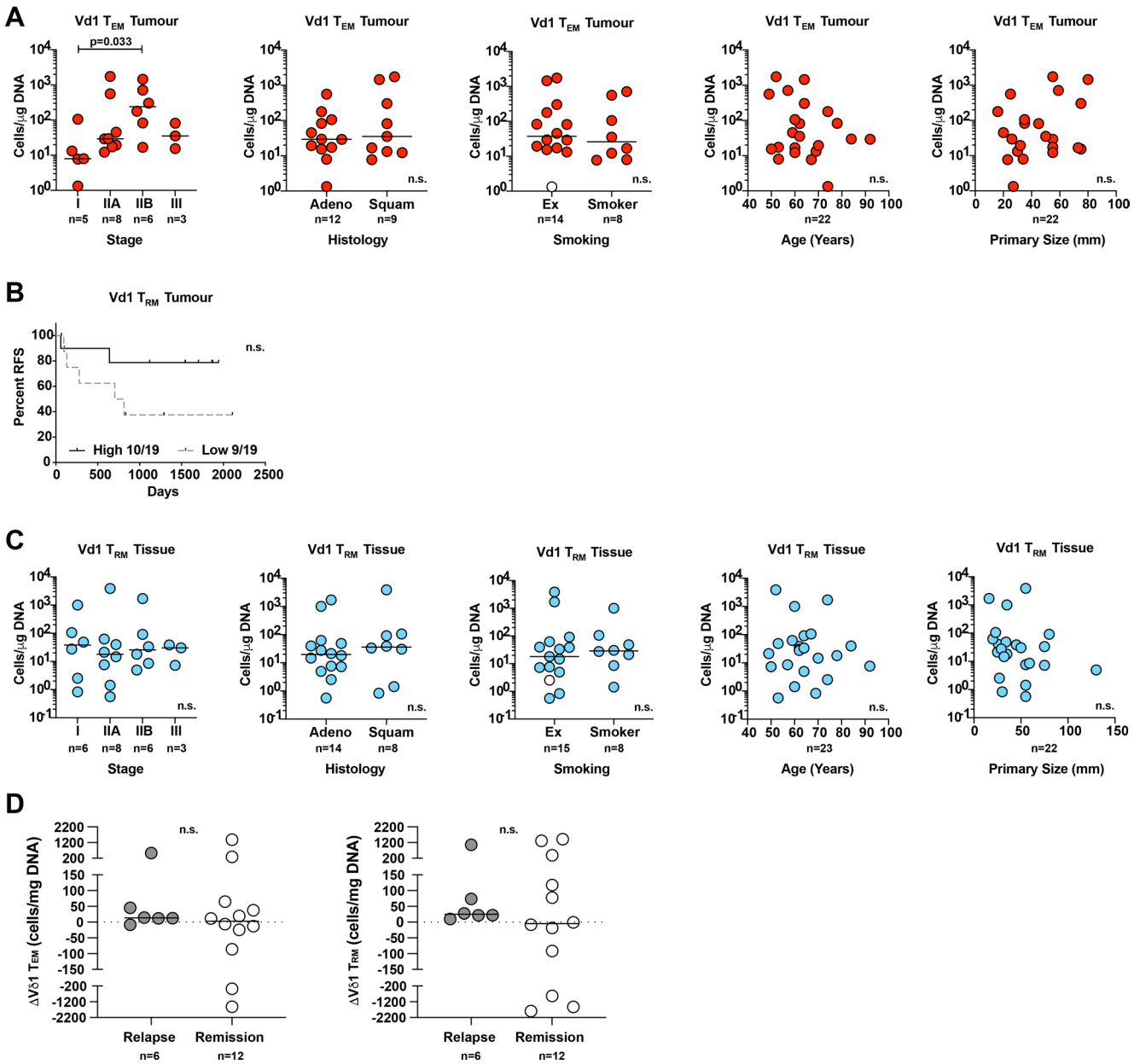

Extended Data Fig. 8 | Prognostic value of Vδ1 T cells is largely independent of other prognostic clinicopathological features. A) Absolute numbers of Vδ1 TEM cells in tumours plotted by TNM stage, histology and smoking status (never smoker, unfilled circle) as well as against age and primary size. Kruskal Wallis with post hoc Dunn's test corrected for multiple testing (stage). Bar=median. Mann-Whitney test (histology and smoking status). Spearman correlation (primary size and age). **B)** Relapse free survival split on median absolute numbers of Vδ1 Trm cells in tumours. Gehan-Breslow-Wilcoxon test. **C)** Absolute numbers of Vδ1 TEM cells in NT tissues plotted by TNM stage, histology and smoking status (never smoker, unfilled circle) as well as against age and primary size. Bar=median. Kruskal Wallis with post hoc Dunn's test corrected for multiple testing (stage). Mann-Whitney test (histology and smoking status). Spearman correlation (primary size and age). **D)** ΔVδ1 TEM cells (absolute Vd1 TEM cells in tumour - absolute Vd1 TEM cells in paired NT tissue) and ΔVδ1 TRM cells (absolute Vd1 TRM cells in tumour - absolute Vd1 TRM cells in paired NT plotted by outcome. Bar=median. Mann-Whitney test. N numbers and datapoints represent independent patients.

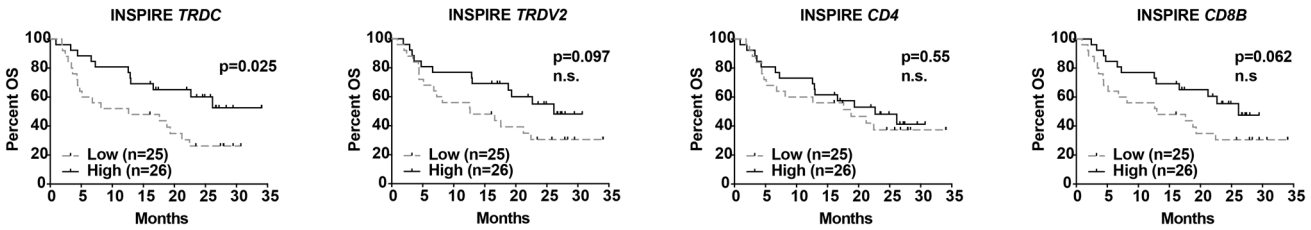

Extended Data Fig. 9 | Association of survival with signature T cell lineage genes in the INSPIRE Trial. Overall survival of patients with advanced solid cancers (mixed histologies) treated with pembrolizumab in the INSPIRE trial. Survival split on median TRDC, TRDV2, CD4 and CD8B expression in primary tumour prior to pembrolizumab. Plotted in months after third cycle of pembrolizumab. Gehan-Breslow-Wilcoxon test. Significant p values shown. n.s. not significant.

nature portfolio

Corresponding author(s): Yin Wu
Adrian Hayday
Charles Swanton

Last updated by author(s): Mar 30, 2022

Reporting Summary

Nature Portfolio wishes to improve the reproducibility of the work that we publish. This form provides structure for consistency and transparency in reporting. For further information on Nature Portfolio policies, see our Editorial Policies and the Editorial Policy Checklist.

Statistics

For all statistical analyses, confirm that the following items are present in the figure legend, table legend, main text, or Methods section.

n/a	Confirmed
☐	☒ The exact sample size (*n*) for each experimental group/condition, given as a discrete number and unit of measurement
☒	☐ A statement on whether measurements were taken from distinct samples or whether the same sample was measured repeatedly
☐	☒ The statistical test(s) used AND whether they are one- or two-sided *Only common tests should be described solely by name; describe more complex techniques in the Methods section.*
☐	☒ A description of all covariates tested
☐	☒ A description of any assumptions or corrections, such as tests of normality and adjustment for multiple comparisons
☐	☒ A full description of the statistical parameters including central tendency (e.g. means) or other basic estimates (e.g. regression coefficient) AND variation (e.g. standard deviation) or associated estimates of uncertainty (e.g. confidence intervals)
☐	☒ For null hypothesis testing, the test statistic (e.g. *F*, *t*, *r*) with confidence intervals, effect sizes, degrees of freedom and *P* value noted *Give P values as exact values whenever suitable.*
☒	☐ For Bayesian analysis, information on the choice of priors and Markov chain Monte Carlo settings
☒	☐ For hierarchical and complex designs, identification of the appropriate level for tests and full reporting of outcomes
☐	☒ Estimates of effect sizes (e.g. Cohen's *d*, Pearson's *r*), indicating how they were calculated

Our web collection on statistics for biologists contains articles on many of the points above.

Software and code

Policy information about availability of computer code

Data collection	No custom code was used to collect data. NSCLC data from TCGA was acquired using R software (version 4.0.2). Gene expression data, Workflow Type: HTSeq-Counts and clinical data from the TCGA-LUAD and TCGA-LUSC projects were downloaded from Genomic Data Commons (GDC) Data Portal using the R/Bioconductor package TCGAbiolinks version 2.16.4. BD FACSDiva software was used for collection of flow cytometry data
Data analysis	No custom code was used for data analysis. CCutadapt version 2.10 DESeq2 version 1.28.185 FASTQC version 0.11.5 FASTQC version 0.11.9 GATK version 4.1.7.0 MultiQC version 1.9 QoRTs version 1.3.6 RNA-SeQC version 1.1.8 RSEM version 1.3.0 RSEM version 1.3.3 Somalier version 0.2.7 STAR aligner version 2.5.2 STAR aligner version 2.5.2a Survival version 3.2-13

Trim Galore! utility version 0.4.2
FlowJo version 10
GraphPad Prism version 9.2.0
immunoSEQ Analyzer version 3.0
JMP Pro version 15.0.0

For manuscripts utilizing custom algorithms or software that are central to the research but not yet described in published literature, software must be made available to editors and reviewers. We strongly encourage code deposition in a community repository (e.g. GitHub). See the Nature Portfolio guidelines for submitting code & software for further information.

Data

Policy information about availability of data

All manuscripts must include a data availability statement. This statement should provide the following information, where applicable:

- Accession codes, unique identifiers, or web links for publicly available datasets
- A description of any restrictions on data availability
- For clinical datasets or third party data, please ensure that the statement adheres to our policy

The tumour region RNA-seq data, TCR-seq data, and flow cytometry data (in each case from the TRACERx study), used or analysed during this study are available through the Cancer Research UK & University College London Cancer Trials Centre (ctc.tracerx@ucl.ac.uk) for academic non-commercial research purposes only, subject to review of a project proposal that will be evaluated by a TRACERx data access committee and any applicable ethical approvals, and entering into an appropriate data access agreement. Restrictions apply to the data availability in order to safeguard patient sequence data confidentiality, to ensure compliance with patient study consent, to meet data protection legislation and due to commercial partnership requirements.

Details of all public datasets obtained from third parties used in this study are as follows. Blood Atlas Study (Uhlen et al. 2019, doi.org/10.1126/science.aax9198) transcriptomic data was downloaded from https://www.proteinatlas.org/about/download. GTEx (www.gtexportal.org/) Analysis Release V8 was accessed via dbGaP Accession phs000424.v8.p2. INSPIRE trial (NCT02644369) transcriptomic data were downloaded as SourceData_Fig4.zip from Yang et al. 2021, doi.org/10.1038/s41467-021-25432-7. TCGA human LUAD and LUSC transcriptomic data were downloaded directly using the TCGAbiolinks R package derived from TCGA repository https://portal.gdc.cancer.gov/.

Source data are available as Source Data files.

Field-specific reporting

Please select the one below that is the best fit for your research. If you are not sure, read the appropriate sections before making your selection.

☒ Life sciences ☐ Behavioural & social sciences ☐ Ecological, evolutionary & environmental sciences

For a reference copy of the document with all sections, see nature.com/documents/nr-reporting-summary-flat.pdf

Life sciences study design

All studies must disclose on these points even when the disclosure is negative.

Sample size	Samples (n=25) were chosen based on the availability of banked TILs from NT lung tissue and paired tumours, region-matched bulk DNA, and from patients with at least one follow-up visit after surgical resection. Where available, banked contemporaneous PBMCs were also immunophenotyped by flow cytometry. No other selection criteria were applied.
Data exclusions	Three patients were excluded from outcome analysis due to incomplete surgical resection of their primary tumours.
Replication	Survival outcome was validated in a cohort of 800+ patients with non-small cell lung cancer in the TCGA database. Technical replicates for flow cytometry, TCR sequencing, RNA sequencing and in vitro activation assays were not performed due to the limited availability of material. Biological replicates from multiple independent donors cross-validated the presence of gamma-delta T cell subsets and their phenotypes in clinical samples.
Randomization	Non-interventional study, not applicable
Blinding	Non-interventional study, not applicable

Reporting for specific materials, systems and methods

We require information from authors about some types of materials, experimental systems and methods used in many studies. Here, indicate whether each material, system or method listed is relevant to your study. If you are not sure if a list item applies to your research, read the appropriate section before selecting a response.

Materials & experimental systems

n/a	Involved in the study
☐	☒ Antibodies
☒	☐ Eukaryotic cell lines
☒	☐ Palaeontology and archaeology
☒	☐ Animals and other organisms
☐	☒ Human research participants
☐	☒ Clinical data
☒	☐ Dual use research of concern

Methods

n/a	Involved in the study
☒	☐ ChIP-seq
☐	☒ Flow cytometry
☒	☐ MRI-based neuroimaging

Antibodies

Antibodies used

Anti-CD3 (PerCP-Cy5.5) Biolegend Cat# 317336 Dilution 1:100
Anti-CD4 (PE-Dazzle594) Biolegend Cat# 317448 Dilution 1:100
Anti-CD8a (AF700) Biolegend Cat# 300920 Dilution 1:100
Anti-CD14 (PE-Cy7) Biolegend Cat# 367112 Dilution 1:100
Anti-CD19 (AF700) Biolegend Cat# 363033 Dilution 1:100
Anti-CD25 (BV650) Biolegend Cat# 302634 Dilution 1:100
Anti-CD27 (BV786) BD Biosciences Cat# 563327 Dilution 1:100
Anti-CD45 (BV605) Biolegend Cat# 304042 Dilution 1:100
Anti-CD45RA (BV510) Biolegend Cat# 304142 Dilution 1:100
Anti-CD56 (APC) Biolegend Cat# 362504 Dilution 1:100
Anti-CD103 (BV421) Biolegend Cat# 350214 Dilution 1:100
Anti-CD107A (BV650) Biolegend 328637 Dilution 1:400
Anti-IL-17 (APC) Biolegend 512333 Dilution 1:100
Anti-IFNγ (BV421) Biolegend 502531 Dilution 1:100
Anti-TCR Vδ1 (FITC) ThermoFisher Cat# TCR2730 Dilution 1:100
Anti-TCR Vδ2 (PE) Biolegend 3Cat# 31408 Dilution 1:100
Anti-TCRγδ (PE-Cy7) Beckman Coulter Cat# B10247 Dilution 1:100
Zombie NIR Viability Dye Biolegend Cat# 423106 Dilution 1:500

Validation

Antibodies and reagents used have been validated by commercial suppliers and validation statements can be found on suppliers' websites.

Biolegend
https://www.biolegend.com/en-us/quality/quality-control
"All of our products undergo industry-leading rigorous quality control (QC) testing to ensure the highest level of performance and reproducible results. Each lot is compared to an internally established “gold standard” to maintain lot-to-lot consistency. We also conduct wide-scale stability studies to guarantee an accurate shelf-life for our products. Additionally, we test the majority of our products on endogenous cells rather than transfected or immortal cells that may overexpress the analyte. We assess our reagents with samples and protocols that reflect our customers' experience. Our willingness to monitor the quality of our reagents extends beyond our lab and into yours."

BD Biosciences
https://www.bdbiosciences.com/en-gb/products/reagents/flow-cytometry-reagents/research-reagents/quality-and-reproducibility
"BD Biosciences not only develops its own antibodies but also collaborates with research scientists around the world to license their antibodies. We provide accessibility to the flow cytometry community by conjugating antibodies to a broad portfolio of high-performing dyes, including our vastly popular portfolio of BD Horizon BrilliantTM Dyes. A world-class team of research scientists helps ensure that these reagents work reliably and consistently for flow cytometry applications. The specificity is confirmed using multiple applications that may include a combination of flow cytometry, immunofluorescence, immunohistochemistry or western blot to test a combination of primary cells, cell lines or transfectant models. All flow cytometry reagents are titrated on the relevant positive or negative cells. To save time and cell samples for researchers, pre-titrated test size reagents are bottled at an optimal concentration, with the best signal-to-noise ratio on relevant models."

Beckman Coulter
https://www.mybeckman.uk/reagents/coulter-flow-cytometry
"Our portfolio of Flow Cytometry reagents, entirely manufactured under good manufacturing practices (GMP), covers major application areas including hemato-oncology, HIV analysis, immune monitoring, cell cycle and stem cells studies."

ThermoFisher
https://www.thermofisher.com/uk/en/home/life-science/antibodies/invitrogen-antibody-validation.html
"Part 1—Target specificity verification
This helps ensure the antibody will bind to the correct target. Our antibodies are being tested using at least one of the following methods to ensure proper functionality in researcher’s experiments. Click on each testing method below for detailed testing strategies, workflow examples, and data figure legends.

Knockout—expression testing using CRISPR-Cas9 cell models
Knockdown—expression testing using RNAi to knockdown gene of interest
Independent antibody verification (IAV)—measurement of target expression is performed using two differentially raised antibodies

recognizing the same protein target
Cell treatment—detecting downstream events following cell treatment
Relative expression—using naturally occurring variable expression to confirm specificity
Neutralization—functional blocking of protein activity by antibody binding
Peptide array—using arrays to test reactivity against known protein modifications
SNAP-ChIP™—using SNAP-ChIP to test reactivity against known protein modifications
Immunoprecipitation-Mass Spectrometry (IP-MS)—testing using immunoprecipitation followed by mass spectrometry to identify antibody targets

Part 2—Functional application validation
These tests help ensure the antibody works in a particular application(s) of interest, which may include (but are not limited to):

Western blotting
Flow cytometry
ChIP
Immunofluorescence imaging
Immunohistochemistry
Most antibodies were developed with specific applications in mind. Testing that an antibody generates acceptable results in a specific application is the second part of confirming antibody performance."

Human research participants

Policy information about studies involving human research participants

Population characteristics	This study includes a subset of patients recruited to the TRACERx Study for which population characteristics have previously been reported (DOI: 10.1056/NEJMoa1616288). The population characteristics for the subset of patients included in this study are detailed in Supplementary Table 1
Recruitment	Samples (n=25) for this study were chosen based on the availability of banked TILs from NT lung tissue and paired tumours, region-matched bulk DNA, and from patients with at least one follow-up visit after surgical resection. Where available, banked contemporaneous PBMCs were also immunophenotyped by flow cytometry. No other selection criteria were applied. These criteria may potentially select for larger primary tumours within each stage and results should be interpreted with this in mind.
Ethics oversight	The study was approved by the NRES Committee London - Camden and Islington with the following details: Study title: TRAcking non small cell lung Cancer Evolution through therapy (Rx) REC reference: 13/LO/1546 Protocol number: UCL/12/0279 IRAS project ID: 138871 All participants provided informed consent prior to taking part.

Note that full information on the approval of the study protocol must also be provided in the manuscript.

Clinical data

Policy information about clinical studies

All manuscripts should comply with the ICMJE guidelines for publication of clinical research and a completed CONSORT checklist must be included with all submissions.

Clinical trial registration	TRACERx Lung: https://clinicaltrials.gov/ct2/show/NCT01888601, approved by an independent Research Ethics Committee, 13/LO/1546 INSPIRE Trial: https://clinicaltrials.gov/ct2/show/NCT02644369
Study protocol	TRACERx Lung: The study protocol is available as a supplement to Jamal-Hanjani et al. 2017, https://doi.org/10.1056/NEJMoa1616288 INSPIRE Trial: The study protocol is as a supplement to Yang et al. 2021, https://doi.org/10.1038/s41467-021-25432
Data collection	TRACERx Lung: Clinical and pathological data is collected from patients during study follow up - this period is a minimum of five years. Data collection is overseen by the sponsor of the study (Cancer Research UK & UCL Cancer Trials Centre) and takes place in hospitals across the United Kingdom. A centralised database called MACRO is used for this purpose. Data collection and recruitment commenced April 2014. Recruitment completed at all sites on December 16, 2022 except at London and Manchester hospital sites where recruitment is due to complete March 31, 2022. A full list of all sites for recruitment and data collection can be found in the study protocol (see above). INSPIRE Trial: Patients recruitment and data collection was conducted at Princess Margaret Cancer Centre from March 21, 2016 to May 9, 2018. Data collection cutoff was July 18, 2019. Refer to Yang et al. 2021, https://doi.org/10.1038/s41467-021-25432
Outcomes	TRACERx Lung: disease-free survival is a pre-defined primary endpoint determined by RECIST v1.1 criteria. Last updated June 15, 2021.

INSPIRE Trial: Survival outcomes of the study was defined by progression free survival (PFS) and overall survival (OS). Clinical outcomes was determined by RECIST criteria and clinical benefit was defined as patients with complete or partial response or stable disease greater than 18 weeks. Refer to Yang et al. 2021, https://doi.org/10.1038/s41467-021-25432

Flow Cytometry

Plots

Confirm that:

☒ The axis labels state the marker and fluorochrome used (e.g. CD4-FITC).

☒ The axis scales are clearly visible. Include numbers along axes only for bottom left plot of group (a 'group' is an analysis of identical markers).

☒ All plots are contour plots with outliers or pseudocolor plots.

☒ A numerical value for number of cells or percentage (with statistics) is provided.

Methodology

Sample preparation	Thawed samples were washed in sterile PBS to remove traces of DMSO and serum before staining with Zombie NIR viability dye (1:500 dilution in PBS for 15min/room temperature). Samples were then stained for lineage and differentiation markers for 15 minutes at 4oC (see key reagents table, all antibodies used at 1:100 dilution in FACS buffer), washed twice with sterile 4oC FACS buffer, kept on ice and immediately acquired on a BD LSRFortessa or sorted on a BD FACSAria Fusion. For in vitro activation assays, thawed samples were washed in sterile PBS to remove traces of DMSO and rested overnight in complete RPMI medium (10% FCS + penicillin/streptomycin) at 37oC/5% CO2. Rested cells were seeded at up to 200,000 cells/well in 200mcl of complete RPMI medium the following day. Cells received either no stimulation (complete RPMI medium only) or were stimulated with PMA (10ng/ml) and ionomycin (1mcg/ml). Brefeldin A (5mcg/ml) and anti-CD107A (1:400 final dilution) was added to all wells. Plates were centrifuged at 200g for 2 minutes and incubated at 37oC/5% CO2 for 5 hours. After 5 hours, cells were stained for surface lineage markers as described above. Following surface staining, samples were fixed in BD CellFIX and washed twice with permeabilization wash buffer (Biolegend) before staining for intracellular cytokines (1:100 final dilution of each antibody in permeabilization wash buffer) for 20 minutes at 4oC. Samples were then washed twice with permeabilization wash buffer, resuspended in FACS buffer and immediately acquired on a BD LSRFortessa.
Instrument	BD LSRFortessa or sorted on a BD FACSAria Fusion.
Software	FCS files were analysed using FlowJo version 10.
Cell population abundance	Between 50 and 500 cells were sorted for low input RNA sequencing as detailed in methods.
Gating strategy	Preliminary gates selected cells using an FSC and SSC gate. Doublets were excluded by plotting FSC area versus FSC height and excluding cells outside of a linear correlation. Live leukocytes were gated as CD45-high Zombie-NIR-low single cells. Subsequent gating was as described in supplementary data panels.

☒ Tick this box to confirm that a figure exemplifying the gating strategy is provided in the Supplementary Information.